Tahr Design Proposal

University of Maryland, College Park &
University Carlos III de Madrid

36th Annual Student Design Competition

Sponsored by Airbus

UNIVERSITY OF MARYLAND 18 56

TAHR

UNIVERSIDAD CARLOS III DE MADRID
homo hominis sacra res

Alfred Gessow Rotorcraft Center
Department of Aerospace Engineering
University of Maryland
College Park, MD 20740 U.S.A.

Benjamin Dobson
Undergraduate Student (Team Lead)
bdobson139@gmail.com

Paulo Arias Juarez
Undergraduate Student
pauloariasj@gmail.com

Mohd Hafeez Amry Mohd Abd Hadi
Undergraduate Student
hafmry@gmail.com

Celia Escudero Alcaraz
Undergraduate Student
cescuder@gmail.com

John Lewis
Undergraduate Student
jtlewis529@gmail.com

Kamil Pilaszewicz
Undergraduate Student
kamil@pilasz.com

Narayan V. Pillai
Undergraduate Student
ryanpillai1@gmail.com

Nicholas Zhu
Undergraduate Student
nicholaszhu97@gmail.com

Dr. James Baeder
Professor
baeder@umd.edu

Dr. Vengalattore Nagaraj
Senior Research Scientist
vnagaraj@umd.edu

Dr. Camli Badrya
Assistant Research Scientist
cbadrya@umd.edu

Students will receive credits for ENAE482 (Aeronautical Systems Design) for their contributions

Alfred Gessow Rotorcraft Center
Department of Aerospace Engineering
University of Maryland
College Park, MD 20740 U.S.A.

To the Vertical Flight Society,

The members of the University of Maryland Undergraduate Student Design Team hereby grant the VFS permission to distribute the Executive Summary and Final Proposal for the 36th Annual Design Competition as it sees fit.

Sincerely,

The UMD Undergraduate Design Team

Acknowledgements

The University of Maryland Undergraduate Design Team would like to acknowledge the following faculty for their invaluable knowledge, time, and support. Thank you for an unforgettable final year of undergraduate study.

University of Maryland, College Park

Dr. Vengalattore T. Nagaraj – Senior Research Scientist, Department of Aerospace Engineering

Dr. James Baeder – Professor, Department of Aerospace Engineering

Dr. Camli Badrya – Assistant Research Scientist, Department of Aerospace Engineering

Dr. Inderjit Chopra – Alfred Gessow Professor and University Distinguished Professor, Director of Alfred Gessow Rotorcraft Center, Department of Aerospace Engineering

Dr. Anya Jones – Associate Professor, Department of Aerospace Engineering

Dr. Roberto Celi – Professor, Alfred Gessow Rotorcraft Center, Department of Aerospace Engineering

Industry Professionals

Mr. Charley Kilmain – Manager Mechanical Systems - H1 Program at Bell

Dr. John Tritschler – Director of Research - U.S. Test Pilot School

Brent T. Mills – Mechanical Engineer – Army Research Laboratory

Carlos Delima – Senior Application Engineer – Altair Engineering Inc.

University of Maryland Personnel

Vera Klimchenko
Mrinalgouda Patil
Bumseok Lee
Bharath Govindarajan
William Craig
Wanyi Ng
Emily Fisler
Abishek Shastry
Bernadine Passe

Special thanks to:

Advanced Helicopter Concepts – Frederick
Rogerson Kratos Corporation
Air Zermatt
Maryland State Police Aviation Command – Frederick

Contents

List of Figures

List of Tables

List of Symbols

English Symbols

$\frac{C_T}{\sigma}$	Blade Loading
C_d	Drag Coefficient
C_l	Lift Coefficient
C_P	Power Coefficient
C_T	Thrust Coefficient
C_{P_0}	Profile Power
P	Power

Greek Symbols

α	Aerodynamic Angle of Attack
μ	Advance Ratio
Ω	Rotor Speed
ρ	Air Density
σ	Blade Solidity

Abbreviations/Acronyms

AHP	Analytical Hierarchy Process
AoA	Angle of Attack
BEMT	Blade Element Momentum Theory
BET	Blade Element Theory
FAA	Federal Aviation Administration
FM	Figure of Merit
GTOW	Gross Take-Off Weight
HPEMFC	Hydrogen Proton-Exchange Membrane Fuel Cells
IGE	In Ground Effect
MSL	Mean Sea Level
MT	Momentum Theory
OGE	Out of Ground Effect
RFP	Request for Proposal
RoC	Rate of Climb
SFC	Specific Fuel Consumption
SMR	Single Main Rotor
SPL	Sound Pressure Level

1 Introduction

The task required in the Vertical Flight Society's 36th Annual Student Design Competition, sponsored by Airbus in 2018-19, is to design an "Extreme Altitude Mountain Rescue Vehicle". Specifically, the final product should be able to rescue climbers stranded at 8,870 m (29,100 ft) on a mountain. Although some rotorcraft are known to have good high-altitude performance, none have yet conducted a mission with a meaningful payload at this altitude. Because of this, many climbing hot spots including Mount Everest, leave climbers at the mercy of the elements once they pass a certain altitude.

Mount Everest, the tallest peak in the world, attracts nearly 1,000 climbers each year. Of these, only about 500 successfully complete the task due to the dangerous nature of the climb. While the number of deaths on the mountain has slowly been coming down in recent years, 288 people have died on Everest between 1921 and 2017. Overcrowding at the peak led to 11 deaths in one week in May of 2019. Some of the dangers to climbers include deep crevasses, unpredictable weather, avalanches, rock slides, and lack of oxygen. Many climbers also bring unnecessary equipment making the journey more difficult for the Sherpas who carry their load up the mountain. All these dangers contribute to lives lost ascending the mountain.

Figure 1: The *Tahr* Over Mt. Everest

Helicopters have been used to rescue injured climbers from the side of mountains for many years. However, their capabilities are limited at the highest altitudes. The highest recorded rescue was conducted by an Air Zermatt crew in Nepal at 7,010 m (23,000 ft) in a Eurocopter AS350 (now Airbus H125). This altitude is still about 1,860 m (6,100 ft) lower than the peak of Mount Everest, leaving any injured climbers higher than this altitude at the mercy of the elements. There are more than 100 peaks around the globe taller than 7,010 m (23,000 ft) making rescues on these peaks by helicopter currently unfeasible. This year's goal is to

Tahr Exterior 4-View

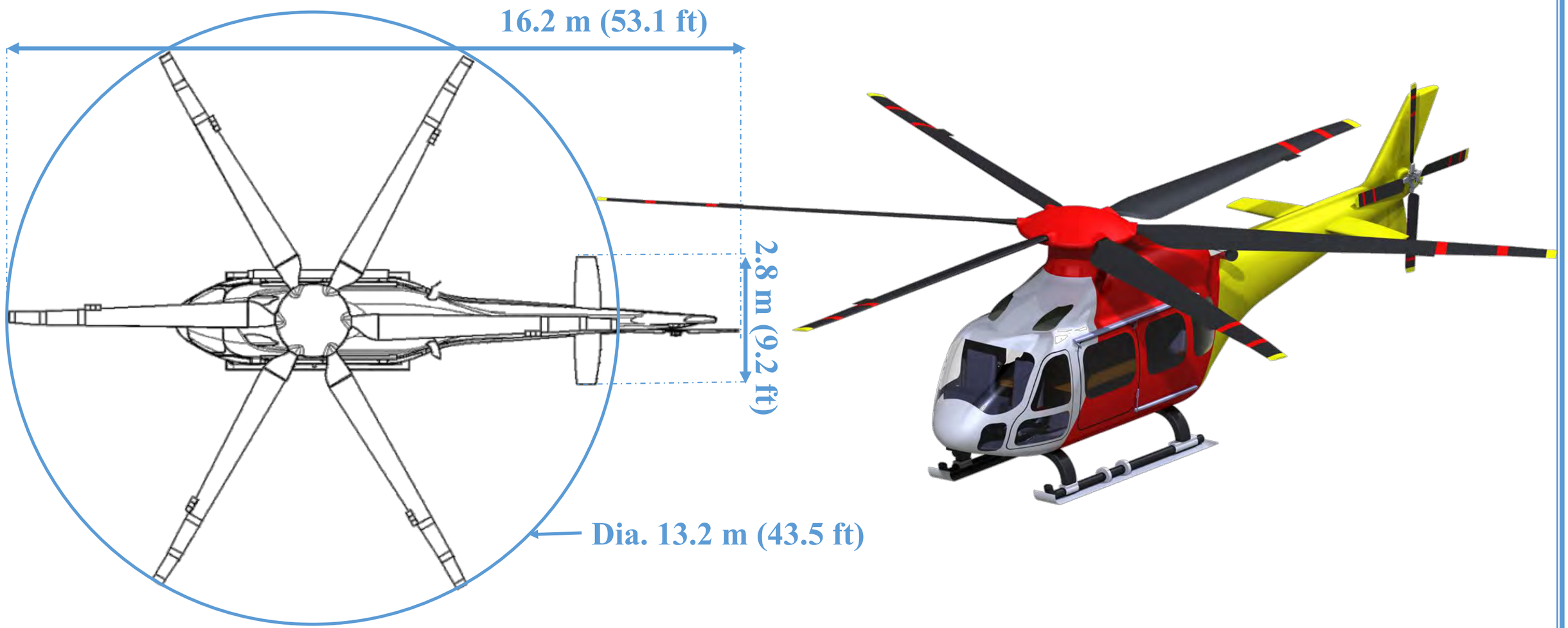

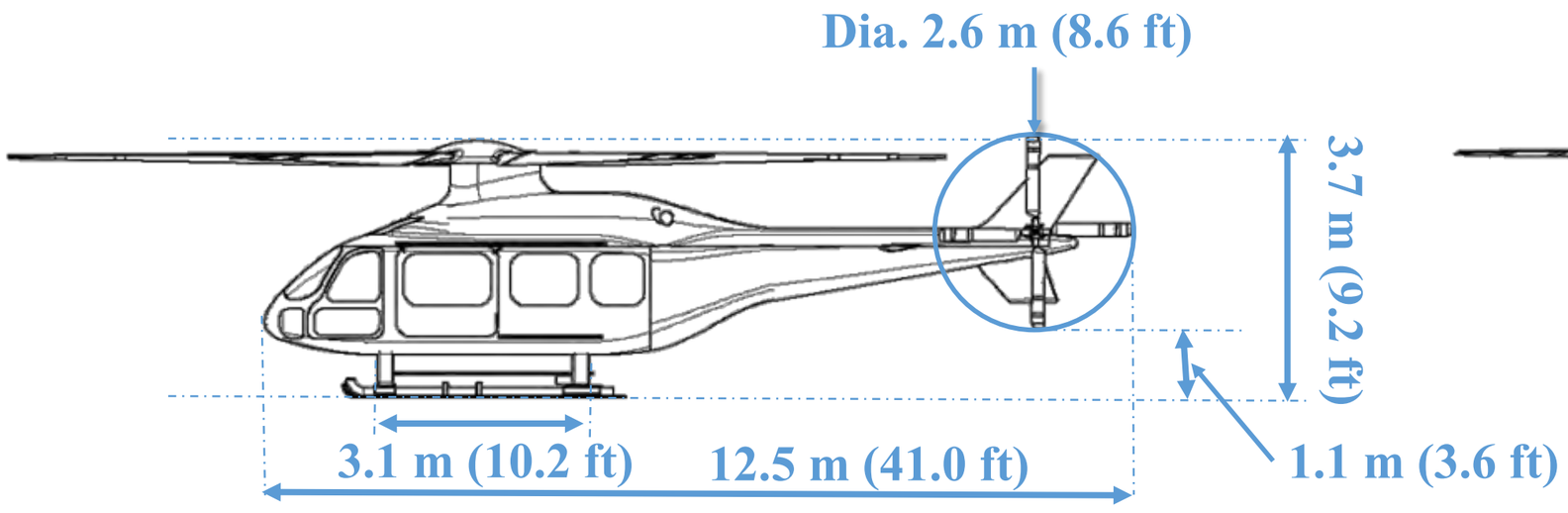

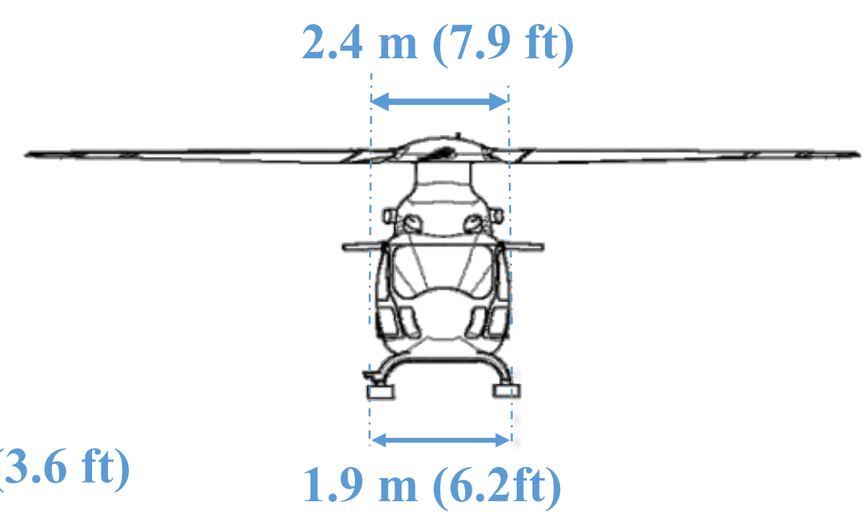

Tahr Key Features

1 **Large interior volume is patient- and worker-friendly**

8 **Aerodynamic fairing houses hingeless rotor hub**

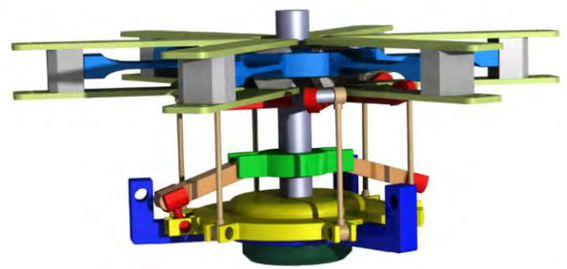

2

Swiveling pilot seats allow any crew member to be involved in rescue

4

Internal hoist extends for smart hoist operation

7

Large tail rotor and empennage provide excellent stability and control

3 **Wide field of view in a pilot-friendly cockpit**

5 **Large main rotor provides high altitude as well as multi-mission capability**

6 **Wide sliding cabin doors facilitate rescue operation**

UNIVERSITY OF MARYLAND

solve this difficulty with an extreme high altitude search and rescue rotorcraft.

In response to this year's RFP, the University of Maryland and Universidad de Carlos III have proposed *Tahr*. The *Tahr* is designed to conduct search and rescue missions higher than any rotorcraft currently available. It utilizes current but innovative technology for reduced procurement costs without sacrificing on quality. Throughout the design process, the team consulted with experienced pilots, rescuers, and mechanics to improve the final design. From this input, *Tahr's* simple design is both cost-effective and versatile in its mission capabilities while being extremely pilot friendly.

Some of the most notable capabilities of the *Tahr* are its high altitude performance, with a hover ceiling of 9,200 meters (30,200 feet) and capable of cruising at 296 km/h (160 kts). For the comfort of any passengers in the *Tahr* it has 6.5 cubic meters (230 square feet) of cabin space. Twin turboshaft engines and a lightweight 3-stage transmission design drives the 6 bladed rotor and allows the *Tahr* to perform any number of missions. And with a state of the art Automatic Flight Control System and Stability Augmentation System the pilots' workload is minimized. Pressurization was also examined to avoid pilots becoming hypoxic. However after detailed discussion with pilots and climbers it was deemed an unnecessary cost and weight and oxygen masks are sufficient.

The *Tahr* is named after the Himalayan Tahr. This mountain goat, though native to Nepal, finds itself comfortably at home in the highest mountain ranges around the world, traversing dangerous terrain with ease. The team was inspired by its ruggedness and majesty. By naming the vehicle after this animal, the team hoped to highlight the high performance of the rotorcraft in many extreme environments.

1.1 RFP Analysis

The specific mission profile in the RFP is composed of three flight legs which must be completed in under three hours. The prescribed mission is a search and rescue mission in an extreme high altitude environment. The details of the individual flight legs are as follows:

- Leg 1: The rotorcraft begins at a large international airport at an altitude of 1,402 m (4,600 ft) at International Standard Atmosphere (ISA) + 20°. The payload at the beginning of the mission consists of 3 crew and EMS equipment totaling 405 kg (893 lbs). After hovering 2 minutes the rotorcraft climbs to 3,780 m (12,400 ft) and flies in a level cruise for 135 km (73 nm) before hovering for 2 minutes and landing at 3,780 m (12,400 ft) with a 10% fuel margin. 20 minutes are then allotted for refueling time. See Figure 2.

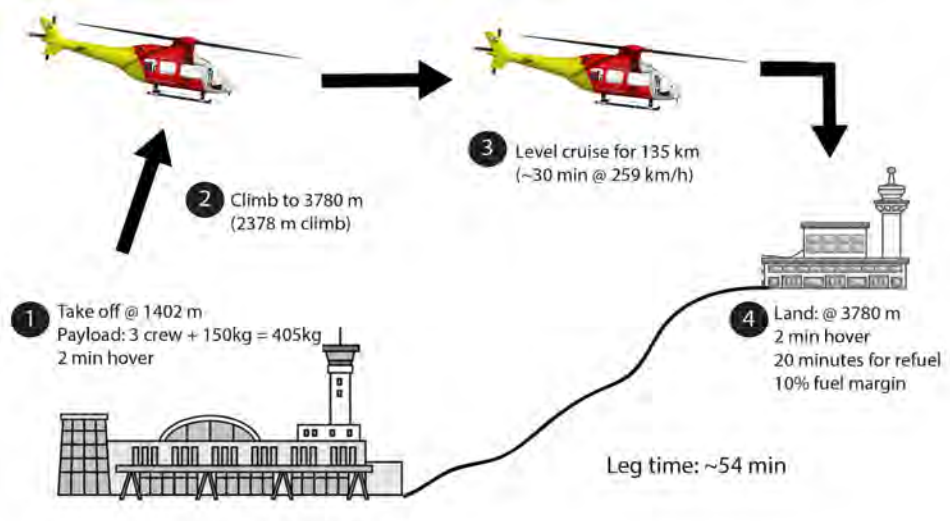

Figure 2: Mission Profile Leg 1

- Leg 2: The rotorcraft takes off from the small airport and hovers for 2 minutes before climbing to 8,870 m (29,100 ft) and conducts a level cruise for 28 km (15 nm) to the rescue site. The rescue is conducted hovering out of ground effect at 8,870 m (29,100 ft) for 30 minutes. During this time, 2 passengers are added, increasing payload to 575 kg (1,268 lbs). The rotorcraft then descends back to the small airport, hovers for two minutes and lands to conduct another refuel for 20 minutes. See Figure 3.

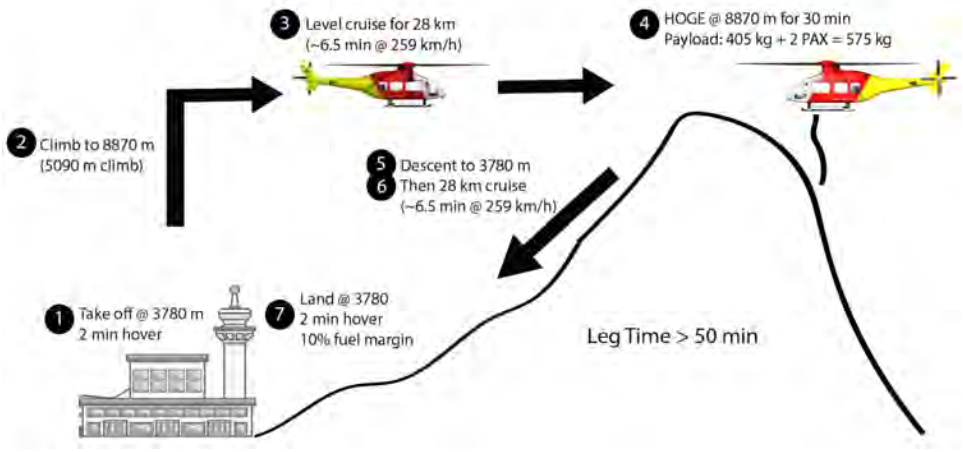

Figure 3: Mission Profile Leg 2

- Leg 3: After an allocated time of 20 minutes for refueling the rotorcraft takes off from the small airport, hovers for 2 minutes, flies at a level cruise of 3,780 m (12,400 ft), descends to 1,402 m (4,600 ft), hovers for 2 minutes and lands to complete the mission at the larger international airport at 1,402 m (4,600 ft). See Figure 4.

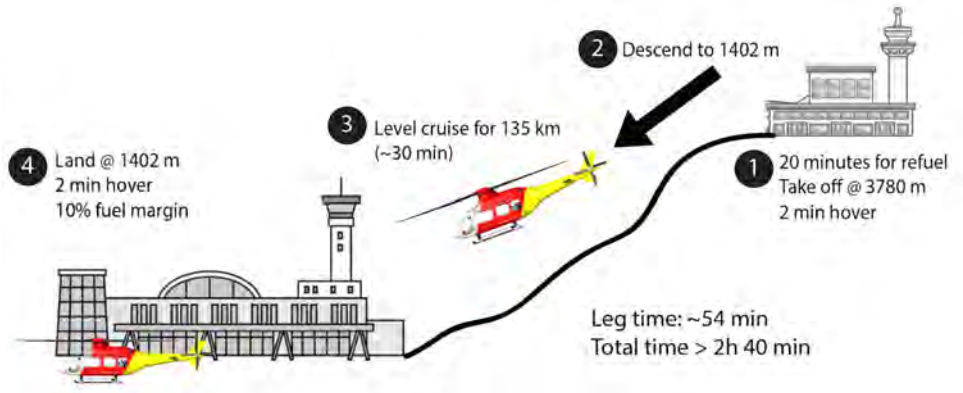

Figure 4: Mission Profile Leg 3

Along with the described mission, these are the following specific design requirements:

- The rotorcraft must be equipped with a hoist system rated for 272 kg (600 lbs) which may be mounted either inside or outside the vehicle.
- The control system (particularly the anti-torque system) must be capable of maintaining heading in hover with winds up to 74 km/h (40 kts) from any azimuth at an altitude of 8,870 m (29,100 ft).

1.2 RFP Compliance

After a thorough review of the RFP, all the requirements were collected into a chart. This ensured that the whole process was driven by exactly what the RFP requested. Table 1 shows which section in the report details the solution for a given requirement.

Table 1: RFP Compliance

RFP Requirement	Design Solution	Section
Hover at 8,870 m for 30 min	SMR configuration including six blades and large rotor and tail rotor diameter, in addition to a light and powerful engine	7.1
Fast Forward Flight	Low weight fuel-efficient twin turboshaft engine, along with low induced and profile drag from the fuselage	6.1
High Controllability	Utilized a simple and compact hingeless rotor hub capable of providing stability and insensitivity to gusts. In terms of navigation systems, Meggitt Helicopter Air Data System (HADS) is included to take real time wind measurements for the GPS system. The Primus 880 Weather Radar allows pilots to avoid turbulent regions	4.3, 9.2.1
Optimized Rotor System	The aerodynamic design of the main and tail rotor was optimized using an in-house code that uses Blade Element Momentum Theory (BEMT) to maximize their Figure of Merit (FM)	4.1, 5.1.1
Optimized Power System	Utilized twin turboshaft RTM322-01/9A engines which provide most optimum specific power available in the market for the rescue mission. This reduces the cost, provides redundancy in case of engine failure, avoids the size effect, and allows for more efficient operation during low power flight	6.1
Hoist System rated for 272 kg (RFP supplement)	Utilized a Goodrich Pegasus Hoist which has a drum design and traction system	10.2.1

2 Configuration Selection

The *Tahr* is a single main rotor aircraft specifically designed for extreme high altitude hover, while maintaining a high factor of safety, forward speed capability, and controllability. Careful attention was paid to the voice of the customer and the design is based closely on the requirements within the RFP. In order to select a configuration which best fits the design requirements, a rigorous process was undertaken to identify possible configurations, compare them, and choose the most suitable configuration.

The process undertaken to obtain the most suitable configuration is as follows. The requirements from the RFP were translated into quantifiable design drivers. After spending the time to define each metric, an analytical hierarchy process was employed to determine the relative importance of each driver; see Section 2.1 for more detail. These weights were then implemented in a Pugh matrix to compare the configurations to one another. From this, a few configurations stood out as warranting further investigation.

Considering a large range of configurations and comparing them to each other highlighted which features would best satisfy the mission requirements. In an effort to gather a variety of options, it was determined that one method of introducing diversity would be to divide the configurations into a number of categories, from which one final configuration would be selected from each. From there, initial sizing of the smaller, unique configurations would be performed to further quantify their relative performance, to result in a final configuration.

(a) VTOL with Transition

(b) Multiple Rotor Aircraft

(c) Coaxial

(d) Single Main Rotor

Figure 5: Final Rotorcraft Categories

To accomplish this, a literature survey on a variety of configurations currently in existence or in conceptual design in industry was performed, then used to determine categories that would be representative of most of these designs. In the end, four categories were defined as shown in Figure 5.

2.1 Analytical Hierarchy Process

The analysis of the RFP in section 1.1 was used to translate the voice of the customer into quantifiable metrics to compare the feasibility of potential configurations. The method involved development of these metrics known as *design drivers*, comparing their relative importance and assigning them weights for use later. The method is known as the Analytical Hierarchy Process (AHP).

2.1.1 Design Driver Formulation

First, each member of the team evaluated the important facets of the mission, arriving at potential design drivers individually. Then, the drivers mentioned were discussed as a team, at which point final design drivers were selected. The team came up with specific definitions as well as metrics of measurement for each. As drivers were defined, similar or drivers of relatively low importance were removed or combined with other drivers. Through the process 19 different drivers were consolidated into 11. The 11 final drivers listed from higher to lower importance are:

- **Safety** - The design must allow for the safest condition for the efficient loading and unloading of injured passengers. Second, the measure of the survivability in the case of mechanical failure. This includes, but is not limited to, autorotative capabilities, one engine inoperability, and crash survivability.
- **Hover Performance** - The ability of the rotorcraft to produce sufficient thrust to hover at 8,870 m (29,100 ft.) for 30 minutes with payload specified by the RFP.
- **Flight Mechanics** - The stability and controllability of the rotorcraft in the presence of 74 km/h (40

kts) wind gusts from any azimuth and its response to changing the center of gravity as specified in the RFP.

- **Cruise Speed** - The highest achievable forward flight velocity above 259 km/h (140 kts), as specified in the RFP.
- **Endurance** - The length of time the rotorcraft can fly without refueling.
- **Payload Fraction** - The fraction comparing payload weight to the takeoff weight of the rotorcraft required by the RFP.
- **Vertical Speed** - The ability of the rotorcraft to climb at a rate of 152.4 m/min (500 ft/min) up to 8,870 m (29,100 ft)
- **Mechanical Simplicity** - The number and complexity of physical components, especially those in motion.
- **Versatility** - The ability of the rotorcraft to conduct a wide variety of mission profiles.
- **Cost** - The life cycle cost of the rotorcraft spanning from development to disposal.
- **Range** - The ability of the rotorcraft to fly for at least 135 km (73 nm) without refueling as required by the RFP.

2.1.2 Analytical Hierarchy Matrix

After specific definitions for each of the drivers were established, they were compared to each other in a decision matrix to determine their relative importance. The relative scoring is as follows. A score of 1, is of "equal importance", 3 is "slightly more important", 5 is "more important", 7 is "significantly more important," and 9 is "absolutely more important." For less important drivers, the scoring uses the reciprocal of these numbers and the terminology remains the same. The diagonals are 1's by default. Scores comparing A vs. B and B vs. A are inverses of each other. The Analytical Hierarchy Matrix arrived at by the team is shown in Figure 6.

Driver	Hover Performance	Cruise Speed	Range	Vertical Speed	Payload Capacity	Endurance	Safety	Cost	Versatility	Flight Mechanics	Mecanical Complexity	Row Sum
Hover Performance	1	3	7	5	3	3	0.33	7	7	1	7	**44.33**
Cruise Speed	0.33	1	7	3	3	1	0.20	7	7	0.33	7	**36.87**
Range	0.14	0.14	1	0.20	0.33	0.20	0.14	1	0.33	0.14	0.33	**3.97**
Vertical Speed	0.20	0.33	5	1	0.33	0.33	0.20	5	5	0.33	3	**20.73**
Payload Capacity	0.33	0.33	3	3	1	1	0.20	5	5	0.33	5	**24.20**
Endurance	0.33	1	5	3	1	1	0.20	5	5	1	5	**27.53**
Safety	3	5	7	5	5	5	1	9	7	1	5	**53.00**
Cost	0.14	0.14	1	0.20	0.20	0.20	0.11	1	1	0.14	1	**5.14**
Versatility	0.14	0.14	3.00	0.20	0.20	0.20	0.14	1	1	0.14	1	**7.17**
Flight Mechanics	1	3	7	3	3	1	1	7	7	1	7	**41.00**
Mechanical Simplicity	0.14	0.14	3	0.33	0.20	0.20	0.20	1	1	0.14	1	**7.36**
Column Sum	**6.77**	**14.24**	**49**	**23.93**	**17.27**	**13.13**	**3.73**	**49**	**46.33**	**5.57**	**42.33**	**271.31**

Figure 6: Design Driver AHP

Figure 1 portrays relative rankings of the design drivers. The bottom row represents the column sums and the right most column is the row sums, which was then normalized, as shown in Table 2, and served as the weights to the Pugh Matrix, which will be further elaborated on in Section 2.2.1.

To highlight the most important design drivers, the highest scores are represented in bold in Table 2. Considering that this is a rescue mission, **safety** will be of the utmost importance. One of the most challenging part of the mission is conducting hover out of ground effect (HOGE) at 30,000 ft with $\frac{1}{3}$ the atmospheric density, implying that **hover performance** must be efficient. In addition to efficiency, the vehicle must have adept **flight mechanics** to maintain stability in the face of 74 km/h (40 kts) wind gusts from any azimuth. The **cruise speed** ranks highly as a design priority to retrieve and fly the rescuee from the mountain to the hospital within the "golden hour". The other design drivers ranked lower relative to **safety**, **hover performance**, **flight mechanics**, and **cruise speed**. These drivers were not omitted in the evaluation and design process and played a role in narrowing down a configuration and selecting a design.

Table 2: Final Weights of Design Driver

Driver	**Score**
Hover Performance	**0.167**
Cruise Speed	**0.110**
Range	0.018
Vertical Speed	0.058
Payload Fraction	0.076
Endurance	0.095
Safety	**0.247**
Cost	0.019
Versatility	0.023
Flight Mechanics	**0.162**
Mechanical Simplicity	0.025
Column Sum	1

2.2 Pugh Matrix

2.2.1 Methodology Explained

The method for comparing various configurations used herein is known as the Pugh Matrix. The Pugh Matrix is a methodology for comparing a number of various concepts with respect to how they perform against a set of criteria. The criteria against which the concepts were measured are the design drivers that were developed in Section 2.1. Note that the design drivers were assigned weights so that the relative importance of each will have an impact on the overall scoring.

After identifying the criteria, the next step in the Pugh Matrix process was to define a *control* configuration. This configuration is defined such that it will receive a neutral score for all categories, and all other configurations will receive scores relative to how they perform in each design driver compared to the control at a qualitative level.

In order to properly score the configurations, a scale enabling scores ranging from absolutely worse to absolutely better than the baseline configuration should be implemented. It was decided to range its scoring from -3 to 3; the significance of those scores is tabulated in Table 3.

Using this scoring system, configurations were scored relative to the single main rotor with a conventional tail rotor at a qualitative level, and the AHP normalized design driver weights were used to generate a final score which would serve as a numerical comparison of how well each one met the needs of the customer.

The pugh matrix for the different configurations can be seen in Figure 4. Note that the design drivers define the rows of the matrix, and the columns house the configurations to score. Also note that the weights applied to the drivers come from the AHP process, as mentioned previously and shown in Table 2.

It can be seen that for the baseline configuration (single main rotor), all scores are zero, or neutral. Note here the influence that the weights have on the overall scores.

Table 3: Pugh Matrix Scoring Explained

Score	Description
-3	Absolutely Worse
-2	Significantly Worse
-1	Slightly Worse
0	Equivalent
1	Slightly Better
2	Significantly Better
3	Absolutely Better

(a) Synchropter Helicopter, The Kaman K-MAX

(b) Coaxial with Tail Propeller, Sikorsky S-97 Raider

(c) Compound Helicopter with Pusher Propeller, Airbus RACER

(d) Conventional Single Main Rotor with Tail Rotor, Airbus H125

Figure 7: Final Four Configurations Considered

The Pugh matrix was used to evaluate 19 unique configurations against a single main rotor design. For better comparison, these configurations were categorized into four groups: single main rotors, VTOL with transition, coaxials, and multiple rotors. Then the highest scoring configuration in each category was selected for further investigation. Descriptions of the four highest scoring configurations are below in Figure 7.

Table 4: Pugh Matrix

	SMR	SMR NOTAR	SMR Fenestron	SMR w/ Tip Jet	Coaxial	Coaxial w/ Pusher Prop	Coaxial w/ Dissimilar Rotors	Coaxial w/ Turbojet Thrusters	Synchropter	Tandem	Side by Side Ducts	Multicopter	Tilt-rotor	Tilt-wing	Multicopter tilt-wing	Lift Offset	Compound w/Pusher	Tailsitter
Hover Performance	0	-0.17	-0.17	-0.17	-0.17	-0.17	0	-0.33	0.17	0	-0.17	-0.33	-0.5	-0.33	-0.33	-0.17	-0.17	-0.33
Cruise Speed	0	-0.11	0	-0.11	0	0.22	0	0.33	0	0.11	0.11	-0.22	0.33	0.33	0.22	0.22	0.22	0.22
Range	0	0	0.02	-0.04	-0.02	0	-0.02	0	0	0.02	0	-0.04	0.05	0.05	0.02	0	0.02	0.02
Vertical Speed	0	-0.06	0	-0.06	0.06	0.17	0	0.12	0	0	0.06	0	0.12	0	0	-0.06	0.12	-0.12
Payload Capacity	0	0	0	0	0	0	0	-0.76	0.08	0.08	0	-0.08	0	0	-0.15	0	-0.08	-0.15
Endurance	0	0	0.10	-0.19	0	-0.10	0.10	-0.10	0	0	0	0	0	0.10	-0.10	0	-0.10	-0.10
Safety	0	0	0	-0.74	0	0	-0.25	-0.25	-0.25	-0.25	0	-0.25	-0.74	-0.74	-0.247	0	0.25	-0.74
Cost	0	0	-0.02	-0.04	-0.02	-0.04	0.02	-0.06	-0.02	-0.04	-0.02	-0.02	-0.04	-0.04	-0.02	-0.02	-0.02	-0.02
Versatility	0	0	0	-0.02	0	0.02	0	0	0	0.02	0	-0.05	0.02	0.02	0.02	0.02	0.02	-0.02
Flight Mechanics	0	-0.16	0	-0.32	0.16	0.16	0.16	0.16	0.16	0.16	-0.16	-0.16	-0.32	-0.05	-0.32	-0.32	-0.16	-0.49
Mechanical Simplicity	0	-0.03	0	-0.03	-0.03	-0.05	-0.03	-0.05	-0.03	-0.03	-0.03	0	-0.08	-0.08	-0.05	0	-0.03	-0.03
Totals	**0**	**-0.53**	**-0.07**	**-1.72**	**-0.01**	**0.22**	**-0.01**	**-0.25**	**0.11**	**0.07**	**-0.21**	**-1.24**	**-1.16**	**-1.17**	**-0.96**	**-0.33**	**0.08**	**-1.75**

2.2.2 Synchropter

A synchropter is a helicopter that has two main rotors side by side and tilted with respect to each other. Figure 7a shows the Kaman K-MAX, the only synchropter currently in production.

The design of a synchropter removes the need for a tail rotor by having two counter-rotating main rotors. As such, the necessary 10% power loss for a tail rotor is now fully available to the two main rotors, allowing for improved hover efficiency compared to a single main rotor helicopter. In addition, having two rotors, the synchropter is able to produce more thrust giving it a better payload fraction compared to a single main rotor.

One of the disadvantages to the synchropter is the need for an additional swashplate which increases the lifecycle cost of the helicopter. Safety was decided based on the lateral distance between rotor tips is much larger to achieve a similar rotor area to a single main rotor helicopter. Multiple swashplates and the rotor angles require a more complex design which gave it a negative mechanical simplicity score. Ultimately, this design was not selected as the final design due to it requiring a large rotor span compared with the SMR based on sizing, see section 3.

2.2.3 Coaxial with Tail Propeller

The coaxial with a tail propeller configuration combines coaxial main rotors and a pusher propeller specifically for increased cruise speed. Figure 7b shows Sikorsky S-97 Raider which implement the coaxial with tail propeller configuration. Another reason this configuration was considered was to offer an alternative to the traditional side loading door. With no tail rotor, it would have been possible to load patients through the back. However in discussions with Air Zermatt rescue workers, they expressed worries that the CG variations might be too large with rear loading. While this configuration did receive a higher cruise score, the team ultimately decided against it because its hover is not as efficient as the single main rotor.

2.2.4 Compound Helicopter with Pusher Propeller

The concept of a compound helicopter with a tail propeller combines both fixed-wing aircraft and rotorcraft resulting in a configuration with fast forward flight capabilities. Figure 7c shows Airbus Rapid Cost Effective Rotorcraft, RACER which implement this particular configuration. The addition of a lifting surface lowers the power requirements of the main rotor allowing for faster cruise speeds. However, the lifting surface interacts with the wake of the main rotor, decreasing its hover efficiency. In addition, the lifting surface would have to be strategically placed or else it would interfere with the safety of rescuer and victim. For these reasons, the compound with pusher prop was not selected.

2.2.5 Conventional Single Main Rotor with Tail Rotor

The highest scoring configuration in the single main rotor category was the baseline **single main rotor**. Figure 7d shows Airbus H125 which is one of the common model of conventional single main rotor with tail rotor. It was the best in its category due to its slightly better hover efficiency than the others in the group. Because of the hover requirements in the RFP, this driver carried a high weight. The single main rotor is a mechanically simple design which continues to be a standard in the industry. It is a versatile rotorcraft and the only rotorcraft that has successfully landed on the top of Mount Everest, making the single main rotor the winner of its category. Ultimately, safety and hover efficiency drove the selection process and the single main rotor was selected as the final configuration.

3 Vehicle Sizing

The RFP provided a 3-leg mission profile detailed in Section 1.1. For the initial sizing of the rotorcraft, a code was developed following Tishchenko's methodology [1] and simple momentum theory for power estimation for a single main rotor (SMR) and coaxial rotor configurations. Components' weight estimations were calculated using the Aero Flight Dynamics Directorate (AFDD) equations [2]. Figure 8 shows the process used to optimize the vehicle's weight and power in the code.

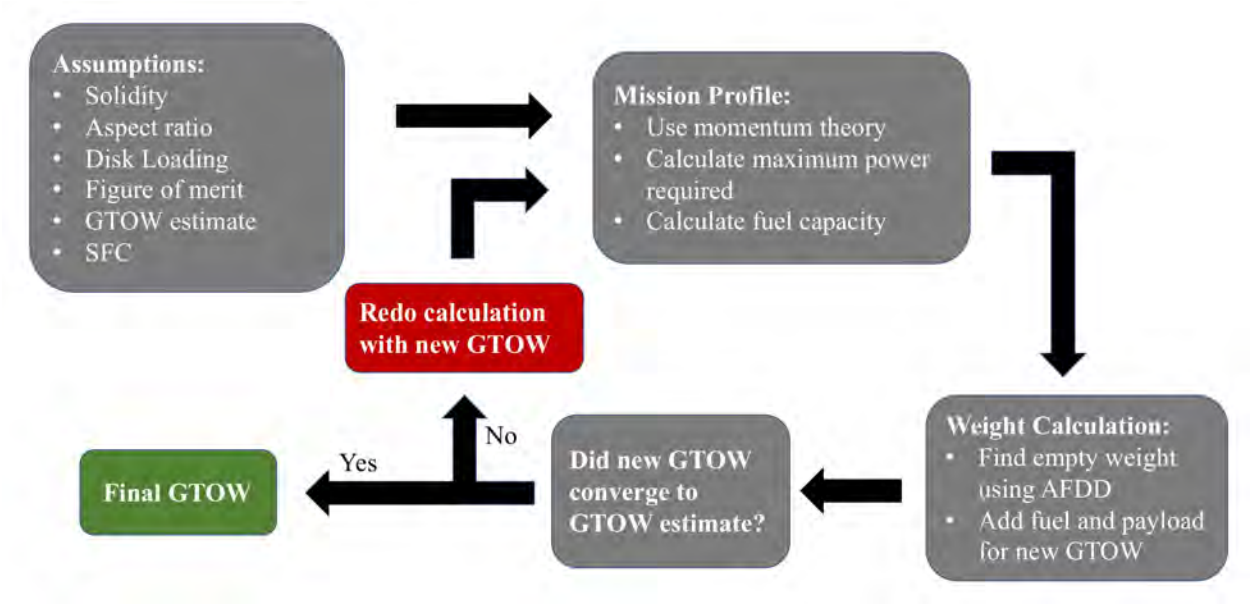

Figure 8: Sizing Code Flowchart

3.1 Methodology

The initial sizing was carried out for a single main rotor and tail rotor helicopter (SMR) and a coaxial configuration. The most important inputs for the code were the number of blades, disk loading, aspect ratio, tip speed, and the cruise and climb velocities. The initial values of these variables were based on already existing rescue helicopters such as the EC-135, then they were optimized for the lowest power, down wash, main rotor diameter, and thrust coefficient through a parametric study. The parametric study consisted of varying the aspect ratio, disk loading, number of blades and tip speed to find the best possible combination. Obtaining the lowest possible blade loading, $\frac{C_T}{\sigma}$, became the priority since it proved the most challenging to obtain a value that does not result in stall at the rescue altitude. The validation of this code is discussed in Section 3.2.

3.2 Code Validation

Since the code was developed by the team members it was necessary to prove that it gives accurate results. The code's aerodynamic analysis was validated against flight test results for the Sikorsky UH-60 Black Hawk.Figure 9 is an example of a comparison of the resulting values of power loading, $\frac{C_P}{\sigma}$, with increasing forward speed when $\frac{C_T}{\sigma} = 0.079$ for the UH-60 Black Hawk.

The momentum theory results in under 10 % error from hover up to $\mu = 0.3$. After this advance ratio the flight test results begin to deviate hinting that the parasitic drag is being underestimated. However the range of advance ratios for which the theory is precise suffices for the scope of our mission and therefore validates

power estimation methodology of the sizing code for forward flight and hover. The AFDD equations [2] used for weight estimations were also successfully validated using a case for the UH-60 found in an NDARC demonstration. [3]

3.3 Sizing Results

In order to finalize the sizing results, several inputs to the code such as the cruise and climb velocities and the characteristics of the engine had to be decided.

The cruise velocity is set to be 296 km/h (160 kts), this yields the best chances to complete the mission in time without substantially increasing the power installed or complicating the blade design to account for high advance ratio. Table 5 shows the time, power and weight implications of assuming various velocities.

Lowering the cruise velocity from 296 km/h (160 kts) only provided a minimal decrease in gross take-off weight and installed power while jeopardizing the three hour mission time.

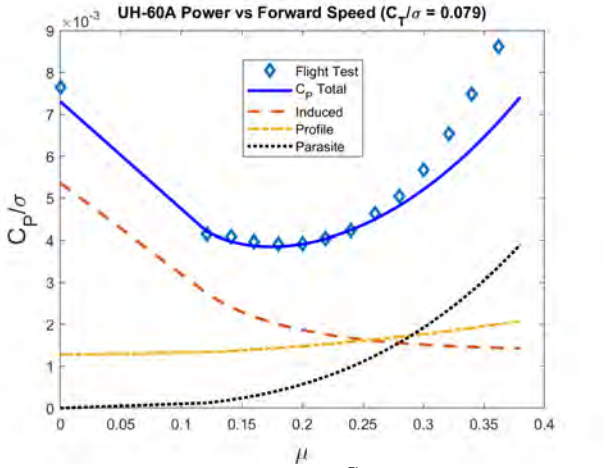

Figure 9: UH-60 $\frac{C_P}{\sigma}$ vs. μ

The rate of climb is set to be 533.4 m/min (1,750 ft/min), this is necessary to climb from 1,402 m (4,600 ft) to 8,870 m (29,100 ft) within a reasonable time frame. This high rate of climb is made possible due to the large amount of excess power the *Tahr* has available in forward flight. The forward velocity in climb and descent is set to be 140 knots. The rate of descent is set to be 304.8 m/min (1,000 ft/min) in order to give the rescuees a comfortable descent. As detailed in Section 6, the specific fuel consumption is 0.30 $\frac{kg}{kW*hr}$ and the power to weight ratio is 6.5 $\frac{kW}{kg}$.

Given the parameters discussed the results indicate that the SMR is the better configuration for the mission since it requires less power and weighs less than the coaxial.

Table 5: Cruise Speed Comparison

Cruise Speed [knots]	GTOW [kg]	Power Installed [kW]	Total Mission Time [min]
140	3,725	2,895	183.7
150	3,726	2,896	179.5
160	3,729	2,899	175.8
170	3,734	2,902	172.5
180	3,739	2,905	169.6

4 Rotor Design

4.1 Main Rotor Aerodynamic Design

The main rotor aerodynamic design was performed with an in-house code that uses Blade Element Momentum Theory (BEMT) to calculate the performance of the rotor in terms of Figure of Merit (FM) and power loading. The airfoils considered were the Clark-Y, MH-60, RC3-8 and RC4-10. A comparison of the $C_l - \alpha$ and $C_d - \alpha$ curves for these airfoils showed that the RC4-10 is the most effective for our mission. The variation of C_l and $\frac{C_l}{C_d}$ with respect to angle of attack (α) for the RC4-10 are shown in Figures 10a and 10b

for four different values of Reynold's number. The red boxes depict the range of α encountered across the span.

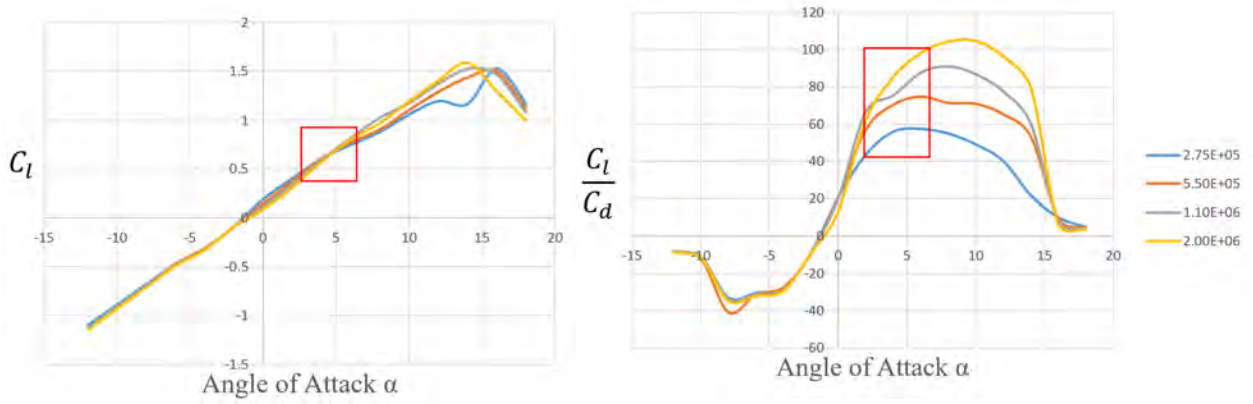

(a) RC4-10 C_l vs. α

(b) RC4-10 $\frac{C_l}{C_d}$ vs. α

Figure 10: C_l and $\frac{C_l}{C_d}$ vs. α at Various Reynold's Numbers

It was decided to use linear pre-twist and taper throughout the blade to improve the rotor performance. Figure 11 shows the parametric study performed in order to find the ideal pre-twist and taper for the blades, the analysis varies taper and twist to find the optimal FM. Although Figure 11 indicates an optimal twist of 18 degrees and 4:1 taper ratio, these values were not chosen due to other considerations. The first of these considerations is that the *Tahr* needs to achieve a speed of 160 knots as well as be capable of hovering efficiently; high twist is detrimental to forward flight and therefore a compromise must be made between low twist and high FM, a pre-twist of 11 degrees at the root was chosen as an appropriate middle value. The second consideration is structural, since the *Tahr* has 6 blades to fit on the rotorhub the root chord has to be small enough that they will fit without risk of collisions due to lead-lag oscillations. A taper of 2.5:1 was chosen in order to account for these structural constraints given the 22% root cut-out chosen to accommodate the hub.

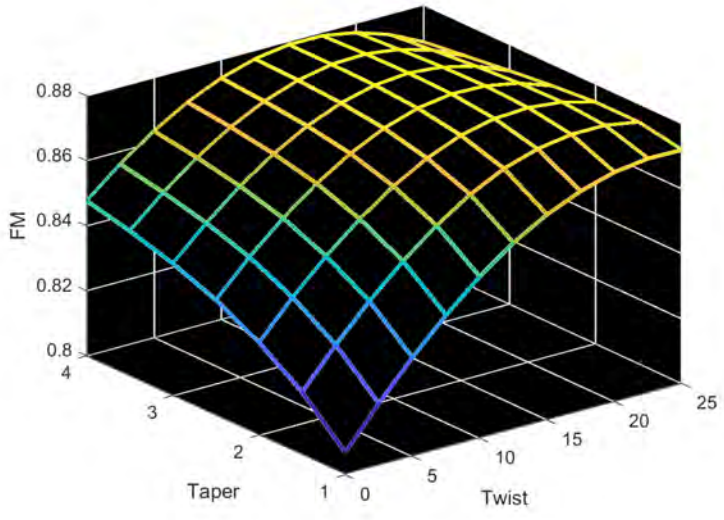

Figure 11: FM vs. Taper vs. Twist in Hover at 8,870 m

The BEMT analysis yielded a rotor that offers a FM of 0.87 at 8,870 m of altitude. The FM depends

increasingly on C_T as altitude increases. This means there is a lower dependency on profile power and therefore the FM value gets closer to a value of $\frac{1}{\kappa}$ than it could at sea level. Table 6 shows the different values of FM, C_T and profile power C_{P_0} compared at sea level and rescue altitude for the rotor with no taper or twist. Figure 12 shows the features of the blade design. Note that a small amount of rear sweep in the outboard section, combined with taper, is used to reduce the normal Mach number.

Table 6: Comparison for Rotor Performance in Hover at MSL and Rescue Altitude, no Taper or Twist

Altitude [m]	C_T	C_{P_0}	$\frac{C_T}{C_{P_0}}$	**FM**
0	0.004	$6.76 * 10^{-5}$	59	0.667
8,870	0.011	$9.41 * 10^{-5}$	118	0.807

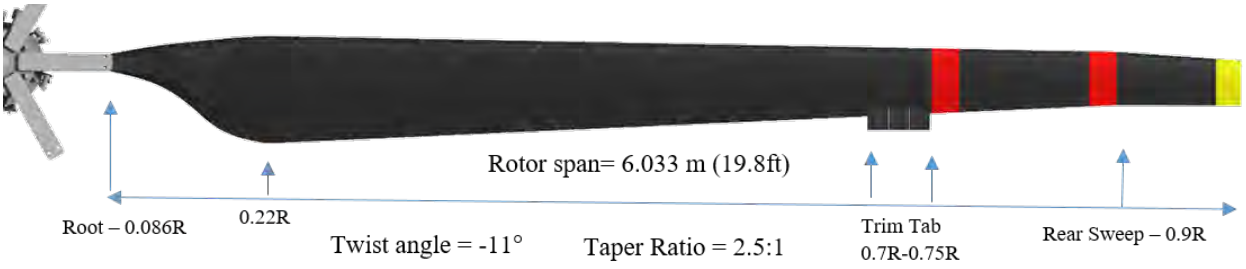

Figure 12: Characteristics of the Main Rotor Blades

4.2 Rotor Blade Structure

The rotor blade structure, as seen in Figure 13, was designed to handle centrifugal forces and flap, lead-lag, and torsional moments alongside shear stresses that the blade will undergo during flight. It consists of three main components: the D-spar and trailing edge block, the graphite composite skin, and the core filling. The D-spar and trailing edge block resist the majority of loads on the blade including centrifugal loads, flap, lead-lag, and torsional moments. The graphite skin provides shear and torsional stiffness. The core filling prevents deformation of the blade skin. A de-icing system as well as lightning protection is critical for safe high altitude operation.

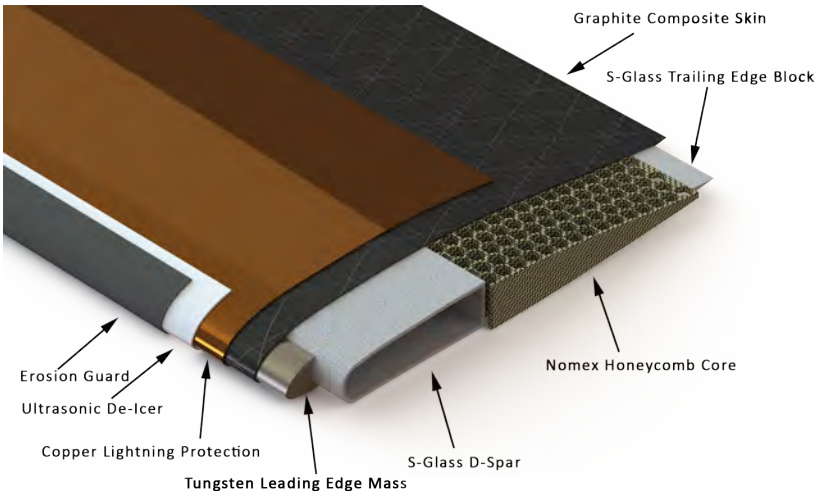

Figure 13: Rotor Blade Internal Composition

4.2.1 Structure Component Materials

For the D-spar and trailing edge block S-glass/epoxy was chosen as it is superior to E-glass in material properties, and in particular its thermal expansion and contraction is lesser than that of E-glass.

For the blade's skin T-300 graphite composite was chosen as the material. In order to ensure the skin retains its shape during flight a core of nomex honeycomb was used.

4.2.2 Composite and Blade Lay-up

The blade's composition was designed in order to achieve the desired flap (EI_y), lead-lag (EI_z), torsional (GJ), and axial (EA) stiffnesses. A leading edge tungsten mass was used to ensure the center of gravity and shear center are located at the quarter chord.

The D-spar is constructed out of unidirectional [0°] layers of S-glass and woven [±45°] torsion wraps made of graphite on the inside and outside of the spar. The graphite skin is constructed of entirely woven [±45°] graphite layers.

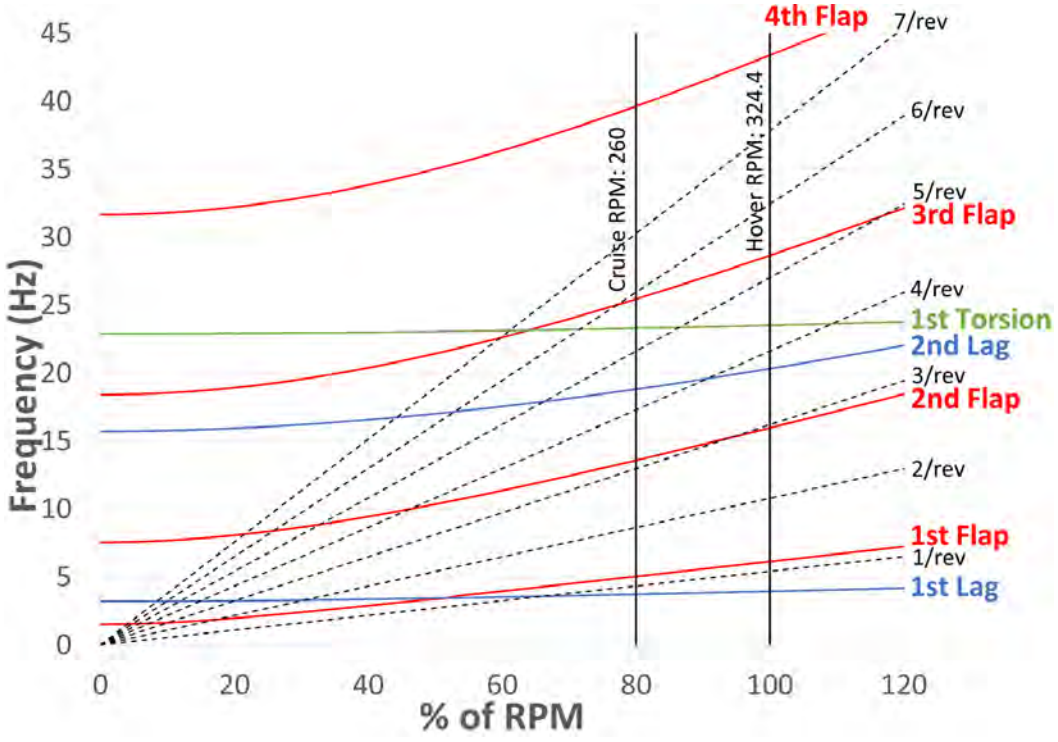

Figure 14: Rotor Blade Fan Plot

The fan plot for the rotor is shown in Figure 14. The stiffnesses were tailored to ensure that the blade frequencies were not close to rotor-order frequencies.

4.2.3 De-Icing

The *Tahr* makes use of a piezo-electric ultrasonic de-icing system located at the leading edge. The micro-vibrations break up the ice that has built up on the leading edge and the flow is able to freely brush it off of the blade. An ultrasonic system was chosen over a thermal de-icer as the ultrasonic system only needs 0.186 W/cm^2 (1.2 W/in^2) while a thermal de-icer requires 4.03 W/cm^2 (26 W/in^2).

4.2.4 Leading-Edge Erosion Guard

Due to the multi-mission requirement of the *Tahr* and expected particulate strikes the rotor blades' leading edges are protected by a nickel protection strip bonded to the blade, with a strip of polyurethane tape along

the metal. This will protect the leading edges from water, sand, and erosion.

4.2.5 Lightning Protection

Due to the requirement that the *Tahr* operate at very high altitudes it is necessary to protect the blades from lightning strikes. This is done by the use of a copper mesh embedded into the graphite skin of the blade that transmits the lightning to a ground point.In order to ensure that the mesh functions properly, the paint on the blades is limited to 9mm thick.

4.3 Rotor Hub Design

In order to select the type of hub used, four types were considered: articulated, teetering, hingeless and bearingless. A similar process to the configuration selection was used to select the hub. First, the design drivers were used to compare the 4 types of hubs in a simple Pugh matrix.

Table 7 shows the process undergone to select the rotor hub. The design drivers are listed at the left and the hubs are listed at the top. The articulated hub was chosen as the baseline and the other hubs compared with it. The scoring system is simply 1 for "better than", 0 for "same as" and -1 for "worse than". It is shown that the hingeless received the highest score.

Table 7: Pugh Matrix for Hub Selection

Drivers	Articulated	Teetering	Hingeless	Bearingless
Control Power	0	-1	1	1
Stability	0	0	1	1
Insensitivity to Gust	0	0	1	1
Vibrations	0	1	0	0
Complexity	0	1	1	0
Sum	**0**	**1**	**4**	**3**

The hingeless rotor hub was selected to provide good control authority, stability as well as to be relatively insensitive to gust. In addition, the design is simple and compact. These capabilities will ensure the *Tahr* will be able to maintain heading in hover with wind from any azimuth up to 74 km/h (40 kts) at 8,870 m (29,100 ft) and be well-controllable in any flight condition. Figure 15 shows the hingeless rotor hub designed for *Tahr*.

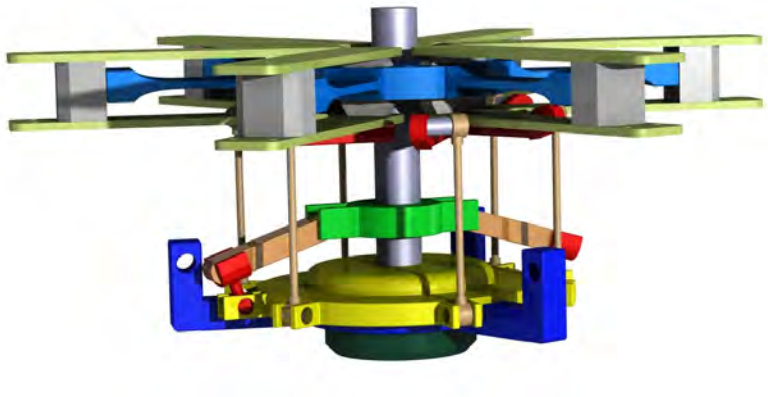

Figure 15: *Tahr*'s Hingeless Rotor Hub Design

The flex beam plays a crucial role in the *Tahr* rotor hub. It provides virtual flap and lead-lag s through the bending and twisting of the composite flex beam. Rigid sleeves on top and bottom of the flex beam form a retention fork for blade attachment. The sleeves also transfer the centrifugal forces from each blade to the center of the flex beam. Therefore, flexible couplings are needed. The inboard end is attached to the thrust bearing while the outboard end is attached to the frequency adapter. Thrust bearing offers flexibility in torsion, flapping and lead-lag articulation. Frequency adapters provide stiffness and damping which allow for the bending and twisting movement. Figure 16 shows the flex beam arm designed for *Tahr*.

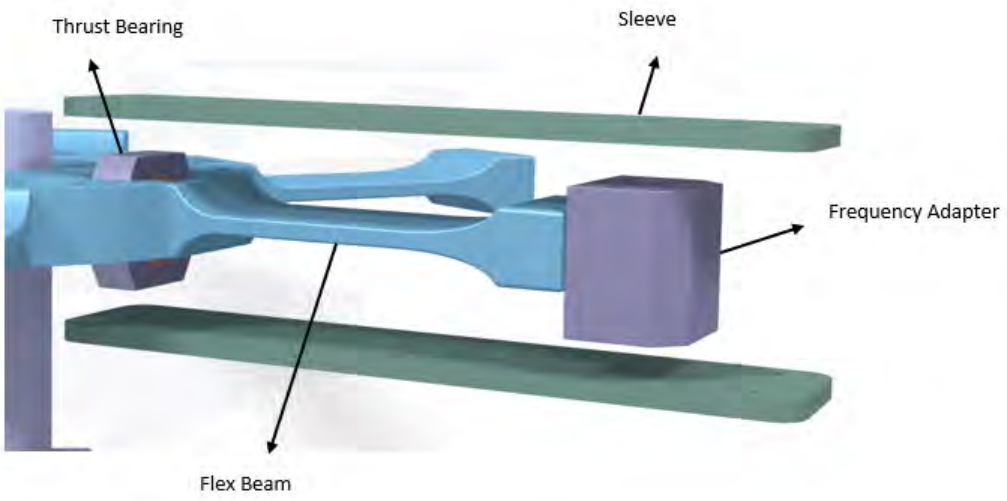

Figure 16: *Tahr*'s Flex Beam Arm

Given the demanding nature of a rescue mission, the rotor hub should be regularly checked and maintained. *Tahr*'s compact and simple rotor hub design make it easier for the ground crew to do a maintenance check and routine. Major components such as frequency adapter and thrust bearing are easy to access on the rotor hub by simply removing the sleeves on the top and bottom of the flex beam. The joint ball bearing can also be easily accessed by removing the non-rotating swashplate for maintenance check and routine.

5 Tail Rotor and Empennage Design

This section explains the design of the tail rotor in detail, as well as empennage features such as the vertical and horizontal stabilizers. These are critical for providing sufficient anti-torque to the main rotor as well as maintaining altitude, orientation, and control.

5.1 Tail Rotor Aerodynamic Design

5.1.1 Sizing

The tail rotor was sized using momentum theory to counteract the torque of the main rotor while hovering at 8,870 m (29,100 ft) and maximum weight. The goal of sizing is to minimize the power required by the tail rotor in hover while maintaining the tail rotor disk area as small as possible.

Trade studies were performed to investigate the effect of various features on the tail rotor power consumption. Table 8 summarizes the parameters studied.

Note that a trendline based on empirical data [4] suggests that for the size of the *Tahr* rotor blades, the expected value is $D_{TR}/D_{MR} \approx 0.17$.

Parameter	Range	Purpose
D_{TR}/D_{MR}	1/8–1/5	P_{TR}/P_{MR}
# of Blades	2–4	C_T/σ
Aspect Ratio	5–9	P_{TR}/P_{MR} & C_T/σ
# of Rotors	1–2	Disk Area

Table 8: Trade Studies Performed for Tail Rotor

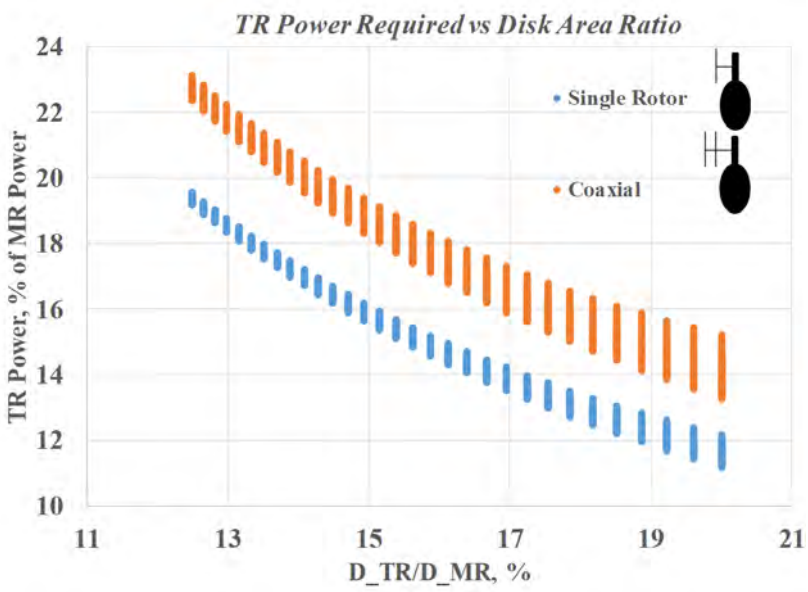

Figure 17: Tail Rotor Sizing Results

Figure 17 shows the result of varying each of these parameters. It is seen that for all the values of diameters, the coaxial tail rotor configuration requires appreciably more power to provide the same anti-torque force. The primary advantage of a coaxial configuration is that it effectively increases the rotor solidity and thus decreases the blade loading. However, the blade loading of a four-bladed single rotor is equivalent to that of a two-bladed coaxial rotor according to Figures 18a and 18b. Furthermore, these figures illustrate that the blade loading falls within a reasonable range of $0.1 \leq C_T/\sigma \leq 0.2$ to prevent stall with appropriate selection of the tail rotor diameter for both single and coaxial rotor configurations. In addition, implementation of a coaxial rotor would increase weight and complexity of the design. Thus, the coaxial tail rotor was eliminated from consideration.

A main result from Figure 17 is that increasing the diameter of the tail rotor decreases the power required. Decreasing the ratio of the main rotor to tail rotor diameter to be less than 5 would further decrease the power required; however, physical limitations on the size of the tail rotor such as ground strikes as well as tendency to enter the vortex ring state caused the tail rotor diameter to be limited to a maximum of one-fifth the main rotor diameter. Using a diameter ratio of $D_{TR}/D_{MR} = 0.2$ saves 26.1 kW (35 HP) of power compared to the empirical result of $D_{TR}/D_{MR} = 0.17$. Given the power loading of the main rotor, this provides an additional 103 kg (227 lb) of potential lifting capability which is enough to lift the entirety of an above-average-size passenger. Therefore, a diameter ratio of 0.2 was selected, resulting in a tail rotor diameter of 2.65 m (8.69 ft).

When the tail rotor is acting in climb, the effective inflow is increased reducing the power requirement providing more operational margin. The selected tail rotor size has an induced velocity at the plane of the rotor disk that is greater than the ambient wind gust of 79 km/h (40 kts). On the other hand, if it is in descent, the induced velocity at the rotor disk plane is higher than the impinging gust of 79 km/h (40 kts)

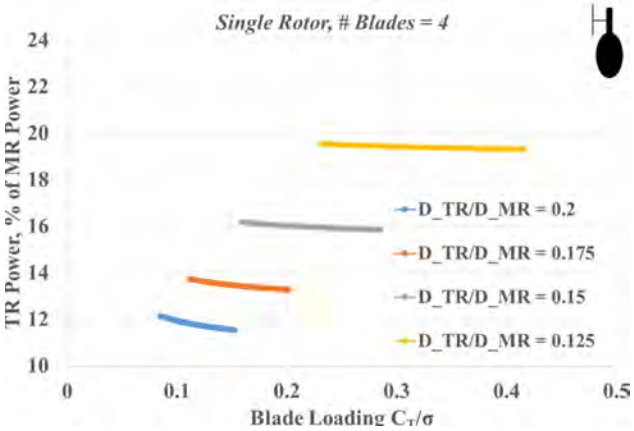

(a) Single Rotor TR

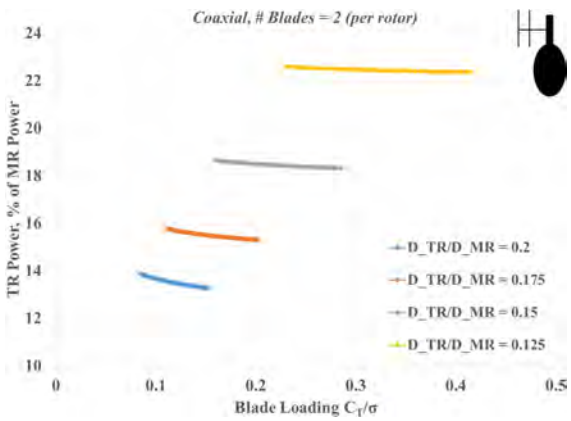

(b) Coaxial Rotor TR

Figure 18: Blade Loading vs. Power Required Comparison of Configuration Considered

which prevents onset of vortex ring state. Note that the tail rotor direction of rotation is such that the tip moves aft at the top, which also delays onset of vortex ring state.

5.1.2 Detailed Design

After deciding on a properly sized tail rotor, refinement of the design needs to be done in order to optimize the aerodynamic performance within the given constraints using BEMT. An in-house code was used to analyze potential combinations of airfoils, twist, and taper in an effort to maximize FM. The tail rotor tip speed was set equal to that of the main rotor, which is 230 m/s (754.5 ft/s) for this analysis.

Airfoil Selection: Six possible airfoils were analyzed during the first step in the design process. No twist or taper were examined during this stage; only the effect of the airfoil on FM at mission altitude was studied. This effect is tabulated in Table 9. It is seen that the Clark-Y airfoil yields the maximum FM at altitude, thus it was selected to be the airfoil across the span of the tail rotor.

Table 9: FM Comparison for Various Airfoils

Airfoil	FM
Clark-Y	0.801
Clark-YH	0.799
Clark-Y-Ref	0.793
MH-60	0.792
RC4-10	0.78
RC3-8	0.768

Taper Ratio: It is well-known that adding taper to blade design can increase FM. However, taper is not typically used for tail rotors because they spin at high rotational speeds and also have smaller chords compared to main rotors. Therefore, there is little room for spars. Inclusion of taper only exacerbates this problem as the chord will be quite small outboard near the tip. Thus, it was decided that the inboard section of the *Tahr's* tail rotor would have no taper. Outboard, however, a taper with ratio 4 was applied to create a swept-back wingtip which would thus reduce the normal Mach number near the tip to reduce compressibility effects.

Twist: Blade twist can be a powerful tool for increasing the efficiency of a rotor. Main rotor blades tend to be highly twisted in an effort to minimize the power required. However, tail rotors are not because they are required to operate in both directions in order to provide directional control. As a compromise between these

two conflicting criteria, the twist of the *Tahr's* tail rotor was limited to 10 degrees of total twist. Maximum FM was achieved with higher levels of twist for all aspect ratios investigated, thus a twist from root to tip of -10 degrees was chosen.

Aspect Ratio: As mentioned earlier, aspect ratios ranging from 5 to 9 were investigated for its effect on FM. Table 10 compares the FM corresponding to each of these aspect ratios for twist of $-10°$. An aspect ratio of 7 provides the maximum FM in this situation, thus it was selected for the *Tahr*.

Table 10: Selection of Aspect Ratio

Aspect Ratio	FM
5	0.842
6	0.845
7	0.845
8	0.844
9	0.842

The finalized design of the tail rotor is tabulated in Table 11 and shown in Figure 19. The tail rotor blades rotate on top from front to back.

Table 11: Tail Rotor Design Features

Airfoil	Clark-Y
Diameter, m (ft)	2.65 (8.69)
Chord, m (ft)	0.19 (0.62)
Aspect Ratio	7
Solidity σ	0.18
FM (sea level)	0.752
FM (rescue altitude)	0.845
DL [N/m^2 (lb/ft^2)]	497 (10.4)
C_T/σ	0.118

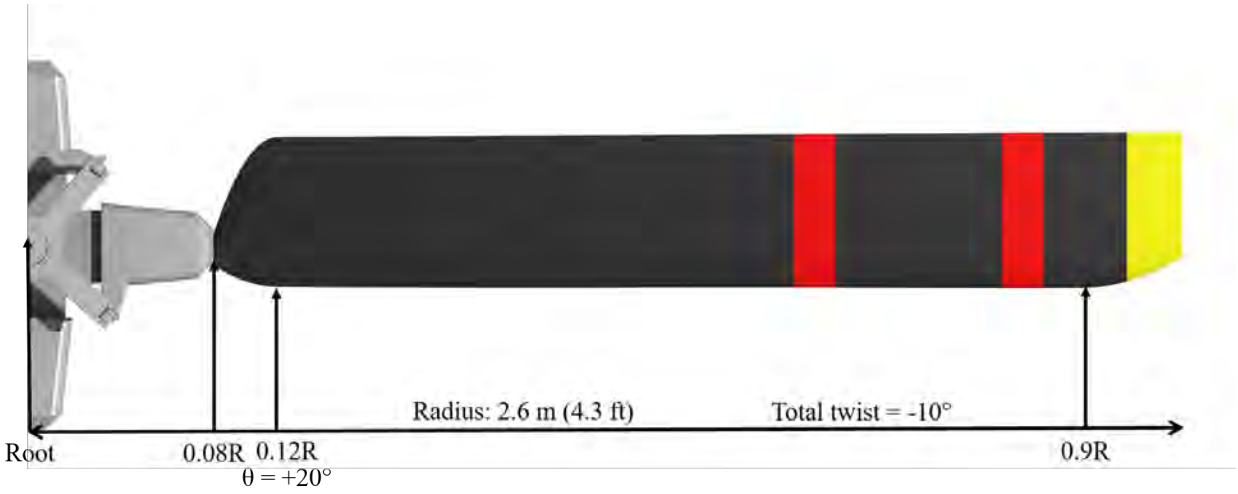

Figure 19: Tail Rotor Design

5.2 Vertical Stabilizer Design

It was decided to size the vertical fin such that the tail rotor can be fully offloaded at the cruise condition specified in the RFP, that is, at 3,780 m (12,400 ft) on an ISA+20 day, and at the *Tahr's* design cruise speed of 296 km/h (160 knts). The lift required by the fin can then be determined by assuming an effective moment arm at which the fin lift vector operates with respect to the center of mass, which was 7.7 m (25.3 ft) for the *Tahr*. Based on the anti-torque requirement, this results in a required sideforce of 3.25 kN (732 lbs).

This requirement is fulfilled by careful selection of the airfoil which thus determines the required planform area of the fin. The airfoil must be selected to be thick enough to house the tail rotor gearbox, but have a low drag. Therefore, a highly cambered, thick airfoil, the NACA 4418, was chosen and installed at zero angle of incidence resulting in a vertical fin surface area of 2.44 m^2 (26.3 ft^2). The aspect ratio of the vertical fin is 1.7 to make it a short and stubby shape which allows for very strong structural support as well as reduces the blockage ratio of the tail rotor. The vertical fin has a taper ratio of the root to tip of 1.5 and a sweepback angle at the quarter-chord of 40° based on empirical data from existing helicopter designs [5].

5.3 Horizontal Stabilizer Design

A horizontal stabilizer is required to ensure stability about the pitch axis in forward flight. The design of the horizontal stabilizer is further complicated for the *Tahr* due to the large diameter of its tail rotor. In fact, the tail rotor is so large that it forces a design decision between an asymmetric tail configuration and a symmetric one. The first, in which the tail rotor is mounted high on the upper fin with the horizontal stabilizer across from it on the opposite side, is shown in Figure 20a. This configuration has three primary advantages:

1. Decreased blockage of tail rotor area by vertical stabilizer
2. Decreased surface area required by horizontal stabilizer
3. Improved safety via increased rotor clearance from ground

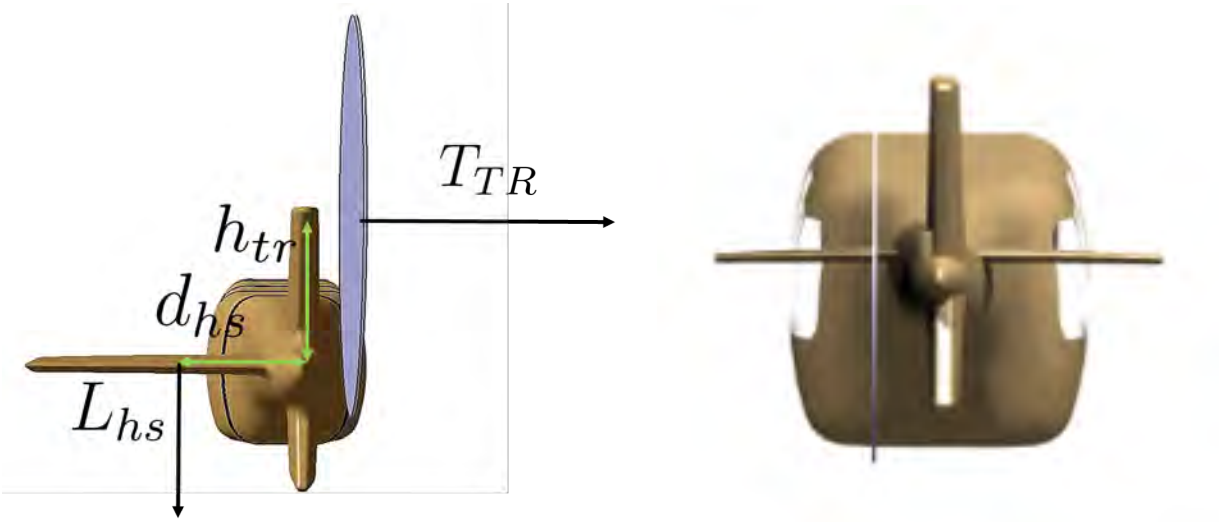

(a) Asymmetric Tail Rotor Configuration

(b) Symmetric Tail Rotor Configuration

Figure 20: Comparison of Horizontal Stabilizer Configurations Considered

Despite these advantages, this configuration greatly increases the design complexity, as the tail rotor thrust vector is no longer aligned with the center of gravity of the helicopter as seen in Figure 20a. This induces

a rolling moment about the center fuselage axis that must be canceled by the horizontal stabilizer. Thus the horizontal stabilizer must be sized to perform multiple functions at the same time. In addition, this configuration requires the tail rotor to be of the "tractor" configuration, meaning its wake accelerates towards the vertical stabilizer, instead of a "pusher" which pushes the wake away from the fin. Pusher tail rotors have been shown to be more efficient [4] so they are preferred if possible.

The alternative would be to decrease the moment arm of the horizontal stabilizer such that it can be placed entirely in front of the tail rotor with half of its required surface area located on either side of the central tail boom, as shown in Figure 20b. This does place the stabilizer in the downwash of the main rotor and fore of the tail rotor, increasing aerodynamic interactions between the three components. However, it simplifies the design by allowing the tail rotor shaft to be lowered to be in line with the tail boom profile thus removing the rolling moment problem. This also simplifies the design of the tail rotor gearbox and drive shaft, since now all components remain in one horizontal plane. The reduction in aerodynamic performance caused by increasing the blockage ratio of the tail rotor is offset by the ability to move the tail rotor to the other side of the vertical fin such that a pusher configuration is achieved.

The symmetric configuration was ultimately chosen because of the resulting design simplification as well as the prominence of forward-mounted horizontal stabilizers on existing, proven helicopter such as the AugstaWestland-109. The stabilizer was sized based on empirical data [4] according to Equation (1) to get an area of 1.19 m^2 (12.8 ft^2). To retain a compact airframe, the span of the stabilizer was limited to 1.2 m (3.94 ft) on either side of the tail boom. A NACA 2412 airfoil was chosen to provide sufficient lift at a small angle of incidence via camber while remaining thin to limit drag penalties.

$$S_h = 0.0086\pi R_{MR}^2 \tag{1}$$

Table 12 summarizes the design parameters for both the horizontal and vertical stabilizers. The finalized designs of the tail features are shown in Figure 21. A negative incidence was chosen to provide a slight download in normal operation.

Table 12: Empennage Design Parameters

Parameter	Vertical Stabilizer	Horizontal Stabilizer
Airfoil	NACA 4418	NACA 2412
Area	2.44 m^2 (26.3 ft^2)	1.19 m^2 (12.8 ft^2)
Span	1.71 m (5.61 ft)	2.4 m (7.87 ft)
Mean Chord	0.91 m (2.99 ft)	0.49 m (1.61 ft)
Aspect Ratio	1.7	4.86
Sweepback Angle	40°	0°
Taper Ratio	1.5	1.5
Angle of Incidence	0°	-5°

5.4 Tail Rotor Hub Design

The tail rotor hub is designed with simplicity and compactness in mind. It consists of two hub plates placed on top of one another. Each end of a hub plate consists of a bearing and torque tube. The torque tube connects the pitch link to the spider. The spider then will be able to move upwards and downwards. This will provide pitch articulation to the tail rotor. Figure 22 shows the tail rotor hub design for *Tahr*.

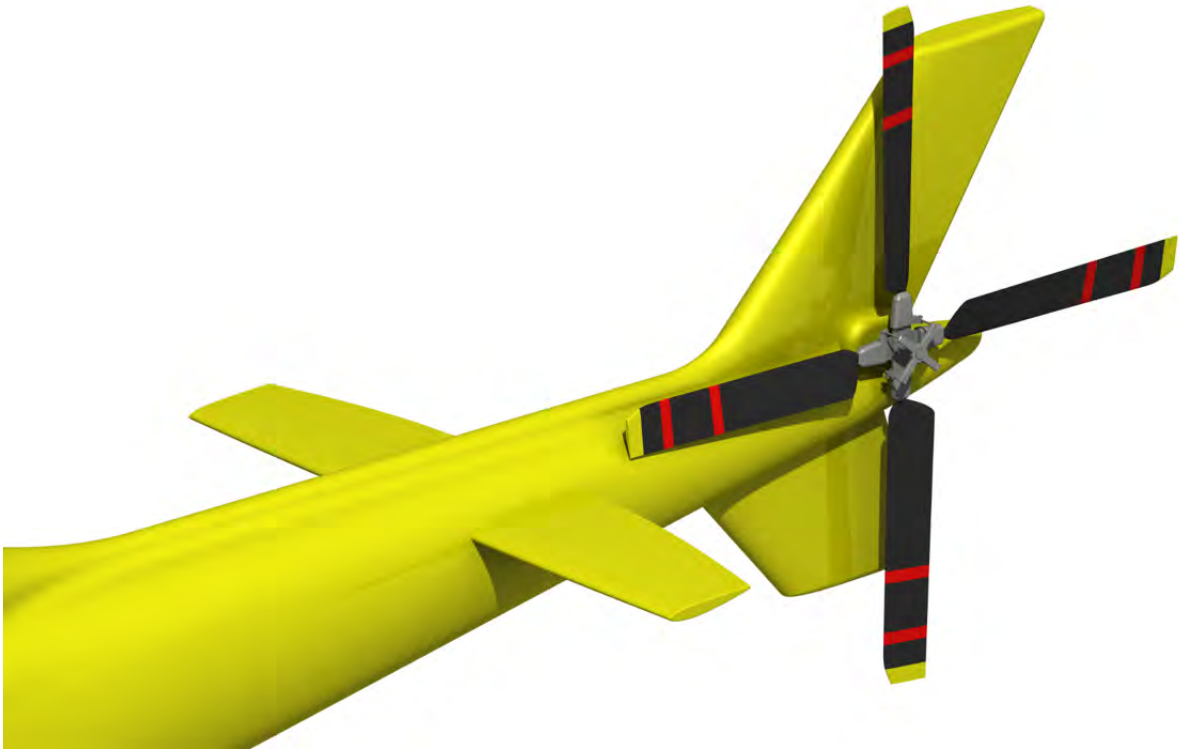

Figure 21: Final Empennage and Tail Rotor Design

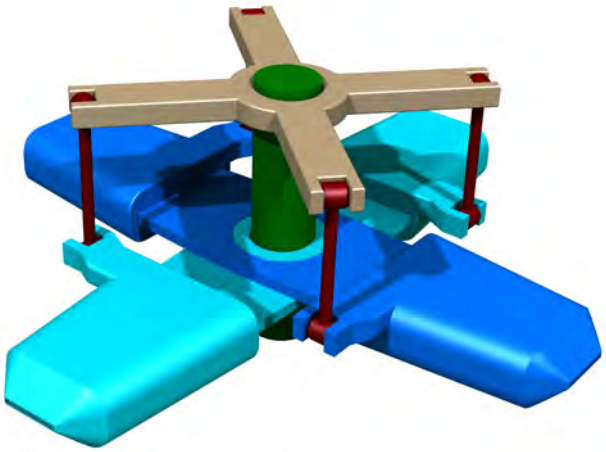

Figure 22: *Tahr*'s Tail Rotor Hub

6 Power Plant System

6.1 Power Plant Selection

A comparison between internal combustion engines and electric engines was performed using the AHP and Pugh Matrix processes. Six types of engines were evaluated: turboshafts, gasoline engines, diesel engines, Lithium-Ion batteries, Aluminum-air batteries, and Hydrogen Proton-Exchange Membrane Fuel Cells (HPEMFC). The design drivers that these were compared by are: power-to-weight ratio, efficiency,

cost, high altitude performance, safety, environmental impact, and ease of maintenance. It was determined that the two primary parameters for selection were specific power and specific fuel consumption, and the values of each for the listed engines can be seen in Table 13.

Modern, high-power Lithium-Ion batteries are limited to specific energy values of approximately 0.18 $\frac{kWh}{kg}$ (278.6 $\frac{Btu}{lb}$), and thus battery weight becomes prohibitively large for the mission. High energy-density Aluminum-Air batteries improve endurance with specific energy values up to 1.80 $\frac{kWh}{kg}$ (2785.9 $\frac{Btu}{lb}$), but because these have a specific power of 200 $\frac{W}{kg}$ (0.122 $\frac{hp}{lb}$) they also become too heavy for the mission. HPEMFC have a specific energy needed of about 0.50 $\frac{kWh}{kg}$ (773.86 $\frac{Btu}{lb}$), and are insufficient for the mission. Both Aluminum-Air batteries and HPEMFC are air breathing engines, which makes their performance decay with altitude as air density decrease.

Table 13: Comparison of Engine Types for Power Plant Selection.

Engine Type	**Specific Power** [$\frac{kW}{kg}$]	**SFC** [$\frac{kg}{kWh}$]	**Advantages**	**Drawbacks**
Turboshaft	4.5-9.0	0.30-0.40	Powerful, compact, very lightweight	High SFC, poor efficiency
Diesel Piston	0.8-1.2	0.20-0.25	Performance at high altitude, reliability, efficiency, low SFC	Low Specific Power
Gasoline Piston	1.0-1.5	0.25-0.35	Reliability, ease of service, low cost	Moderate performance characteristics
Li-Ion	0.25	-	High performance at high altitude, reliability	Very heavy
Al-Air	0.2	-	High specific energy	Very heavy
HPEMFC	0.27	-	High specific energy for long range	Very Heavy, expensive

Although initially electric engines were highlighted for their consistent performance with an increase in altitude, once this analysis was done they were found to be not powerful enough to drive a helicopter up to 8,870 m (29,100 ft). Among the internal combustion engines, turboshaft and diesel piston are the most promising because they present the highest specific power and best performance at altitude. A trade study of over more than 100 commercially available power plants was performed for a baseline comparison.

Figure 23 shows that currently available diesel engines have low power-to-weight ratios and lead to a heavier vehicle for this mission. A turboshaft engine is the only power plant available nowadays that can supply to a rescue helicopter the required power to reach the highest peaks on the Earth, within a reasonable weight. However, the power available from the turboshaft engine reduces with an increase in altitude due to lower air density and engine flow, as shown in Figure 24. Thus, a comparison of the turboshaft shown in Table 14 was done to optimize the performance of the final power plant.

From the listed turboshaft engines the decision was made to use two RTM322-01/9A, as they can supply the required amount of power to accomplish the mission while having an individual weight of 232 kg (441 lb). A comparison between the power required and the power availability is shown in Section 7.1.

Table 14: Comparison of considered Turboshaft Engines

Engine	**GE38**	**AE1007**	**T55-L-714A**	**AL5512**	**RTM322-01/9A**	**T700/T6A1**
MRP/Takeoff Power [kW]	5,516	4,549	3,562	3,039	**1,611**	1,600
Dry Weight [kg]	501	440	399	354	**232**	224
Specific Power [kW/kg]	11.0	10.3	8.9	8.5	**6.9**	7.1
SFC [kg/kWh]	-	0.26	0.32	0.33	**0.26**	-

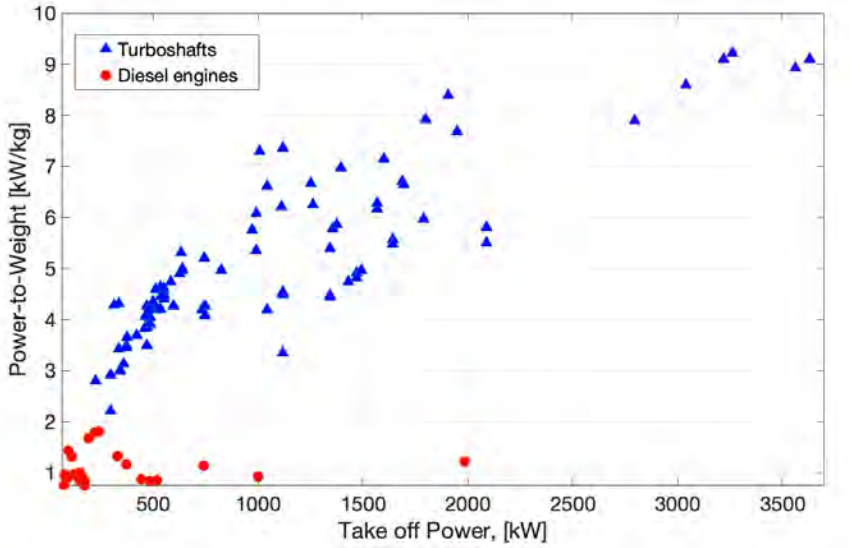

Figure 23: Comparison of Specific Power Values on Turboshaft and Diesel Engines. Database obtained from AARMS (Atlantic Association for Research in the Mathematical Sciences)[6] and EASA (European Union Aviation Safety Agency) certifications

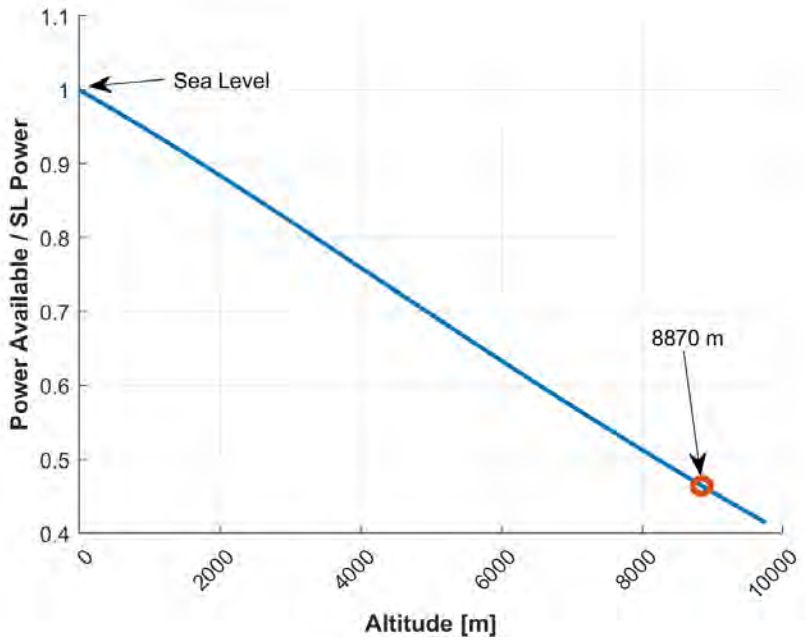

Figure 24: Power Available Decay of a Turboshaft Engine

Both engines are operated at near full power (where turboshaft engines are most efficient) during hover. During lower power flight regimes such as forward flight, one engine can idle while the other provides power at the optimal SFC level. Using this power distribution method, the propulsion system may be tuned to provide the optimal SFC during all flight regimes.

6.2 Transmission Design

6.2.1 Preliminary Steps

The input RPM to the transmission is taken as 6,000 from the manufacturer installed nose gearbox on the engine. The rotor output RPM is 324.4. The maximum amount of power required is 1,306 kW (1,751 hp) and the transmission limit is 1,436 kW (1,926 hp) after adding a margin of 10%.

6.2.2 Configuration Selection

Three configurations were analyzed:

- 1^{st} stage bevel, 2^{nd} stage bevel
- 1^{st} stage bevel, 2^{nd} stage bevel, 3^{rd} stage spur epicyclic
- 1^{st} stage bevel, 2^{nd} stage bevel, 3^{rd} stage helical epicyclic

The gear ratios of each stage were determined using an equation for minimum weight based on stage ratio [7]. Tooth counts for each stage were chosen to satisfy the Hunting Ratio.

6.2.3 Strength and Weight Optimization

The design of the gears followed ANSI/AGMA 2001-D04, ANSI/AGMA 2003-B97, and AGMA 911-A94 standards [8]. An optimization code was written in MATLAB to calculate the volume of the gears based on their face width and diameter and calculate their weight based on the density of each of three materials that were considered. The code would determine the lightest configuration that fell within allowable constraints for bending and contact stresses. From the three configurations it determined that the lightest configuration was the third. The three materials that were analyzed were AISI 9310 Carburized Steel, Grade 2, CarTech Pyrowear 53 Tool Steel, and ATI Allvac Vacso X-2M Steel. Vasco X-2M was chosen as it resulted in the lightest gear weight of 169 kg (372 lb).

6.2.4 Final Design and Construction

The total weight of the transmission including driveshafts, main rotor shaft, housing, oil, etc. is 362 kg (798 lb). The assembled transmission can be seen in Figure 26. The transmission is designed and rated to handle 10,000 hours of operational capacity or 20 years of service, whichever comes first.

6.2.5 Housing

The transmission housing supports the bearings on the shafts holding the gears in the transmission in order to ensure there is no misalignment. The housing is die cast from AZ91D Magnesium Alloy as it is 33% lighter than aerospace grade aluminum and 75% lighter than steel variants and has a superior die life and easier machinability. The housing avoids flat walls which can be excited by the noise produced by the transmission and lead to resonance.

The housing allows both top loading and side loading for the transmission to allow for ease of maintenance.

6.2.6 Lubrication

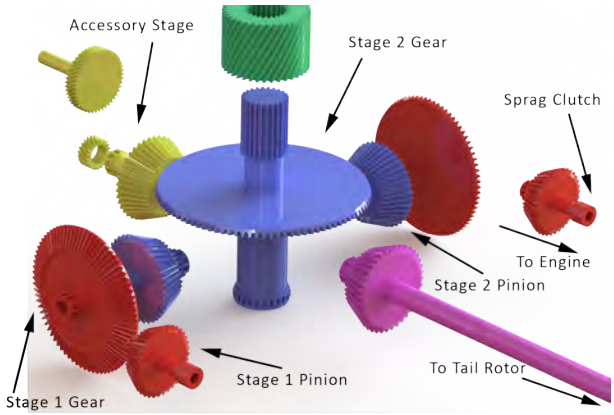

(a) Stages 1 and 2

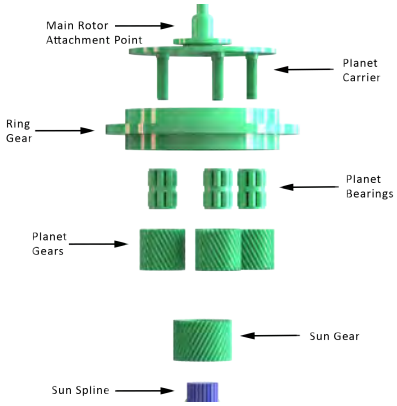

(b) Stages 3 and Main Rotor Shaft

Figure 25: Transmission Exploded Views

The transmission will use MIL-PRF23699F as lubrication and DOD-PRF-85734A as an alternative. Powered by the accessory drive shaft, the oil pump distributes oil via channels built into the housing. Specifically placed nozzles spray the oil onto the gears in order to ensure proper coating. The planet carrier has holes placed in order to improve lubrication ability.

In the event of sub -40 °C weather the transmission can be pre-heated to the operation termperature by a thermal blanket. In this situation it should use MIL-PRF-7808L for lubrication as it is a leaner oil that is better capable of dealing with the extreme cold during startup.

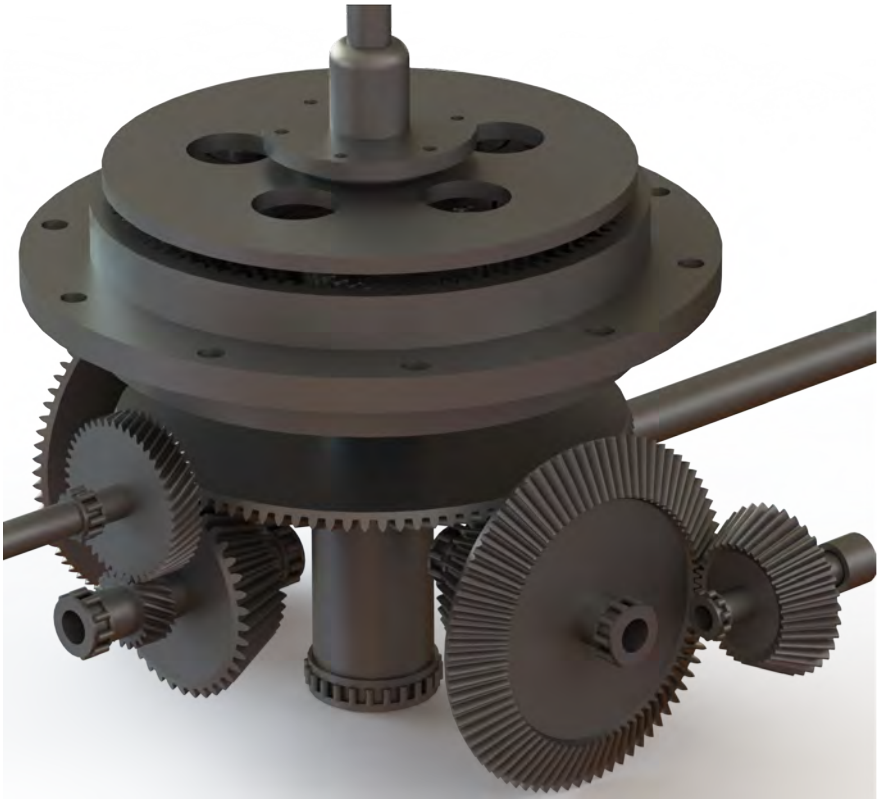

Figure 26: Assembled Transmission

Lubrication channels contain magnetic plugs which are used to collect and separate metal particles from the oil and can be used to detect spalling. This early detection can allow for a transmission repair before a full failure can occur in flight.

In the event of loss of lubrication the system is rated to last for 30 minutes before failure. In order to improve dry-run capability all gears are super-finished and have a low-friction coating. All bearings are grease packed and are made of CBS-600 Caburized Steel, which has good properties for dry-running. A heat exchanger is integrated into the housing of the transmission which further improves dry-run capability as no external piping or fans are required.

6.2.7 Main Rotor Shaft

The main rotor shaft is designed to handle dynamic and static loads and is cast from Titanium 6AI-4V, Grade 5. Above the transmission housing on the shaft is a spline connected to a bearing assembly which holds the lift rod connectors to the shaft and also prevents whirl of the shaft. These lift rods distribute the weight of the rotor assembly while on the ground away from the transmission, and the weight of the vehicle itself during flight. The main rotor shaft is connected directly to the planet carrier through bolts.

6.2.8 Health and Usage Monitoring System

The transmission includes a HUMS system to provide real time diagnostics. Information such as oil pressure, temperature, strain measurements, vibration levels, and chip detection are fed into the flight computer in order to determine the health of the system. In the event of failure the system will alert all operators so that safety measures can be taken.

6.3 Installation of Engine and Transmission

Installation of the engine is a critical consideration because it influences engine performance. Figure 27 illustrates the layout of the engine and associated components. The inlets are located such that they coincide with natural streamlines which occur along the fuselage. They are shaped in a way that allows the flow to expand slightly in order to slow down and become uniform. The exhausts turn the flow exiting the engines to be directly perpendicular to the *Tahr's* long axis such that the hot gases do not affect either the composite tail or main rotor blades. Vibration-absorbing A-frame mounts secure the engines in place on the deck below. Firewalls separate the engines from the transmission and from each other in the event that one of them catches fire. Sand filters are installed to prevent particles from entering and damaging the engines.

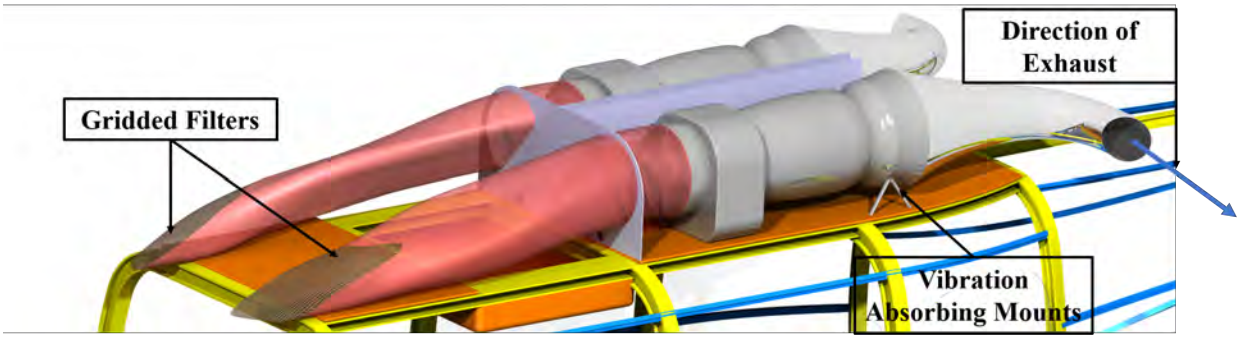

Figure 27: Engine Installation

Figure 28 shows how the transmission is mounted in the airframe; refer to Section 8.1.1 for a description of the associated load paths. Note the location with respect to the inlet is such that the inlet profiles can smoothly pass around the transmission housing and over the engine output shaft to facilitate effective airflow.

7 Performance Analysis

7.1 Hover Performance

The main challenge of this rescue mission is to be able to hover out of ground effect (HOGE) at 8,870 m (29,100 ft) for 30 minutes while the rescue is performed. No existing helicopter is currently capable of achieving this. The challenges of high altitude hover have resulted in some of the unique traits of the *Tahr*

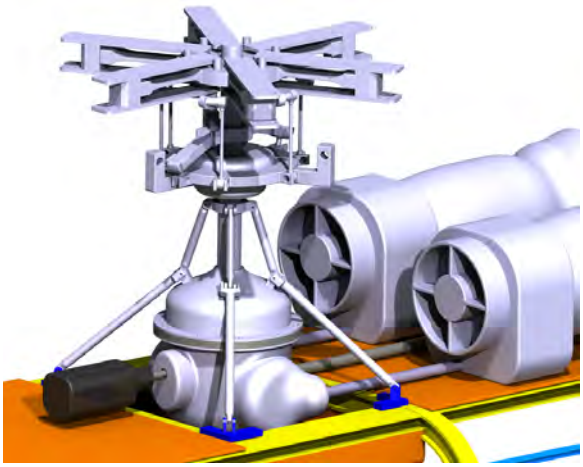

Figure 28: Installation of Transmission in Airframe

including its high solidity and large main rotor and tail rotor diameter. Another important implication has been the powerplant as mentioned in Section 6; this requires an engine that is light and powerful enough that will be capable of delivering the required power even at 8,870 m (29,100 ft.). Figure 29 shows how the power of the selected turboshaft varies with altitude and how this compares to the power required in hover, the *Tahr* has a hover ceiling of 9200 m (30200 ft).

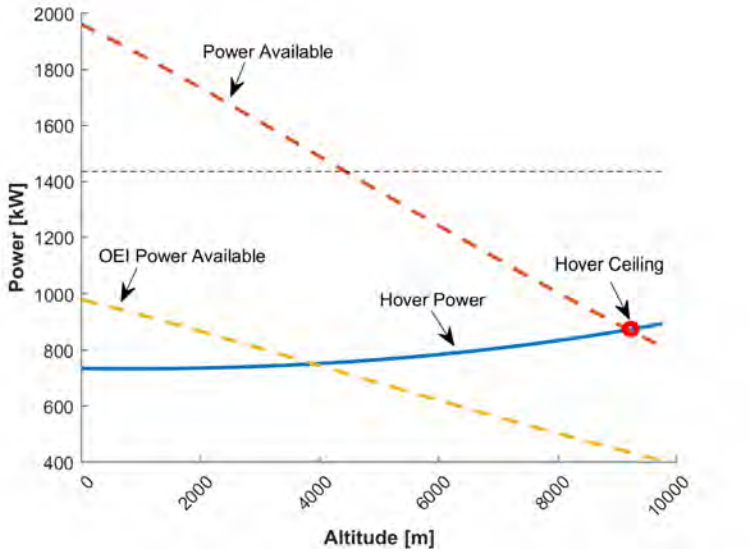

Figure 29: Power Available vs. Altitude, Hover Power vs. Altitude

From Figure 29 it can be seen that even with one engine inoperative (OEI) the *Tahr* is capable of hovering up to 4,000 meters, which is close to the service ceiling of most helicopters.

7.2 Forward Flight Performance

Since the mission is time sensitive and must be completed within 3 hours, forward fight speed capability is almost as important as hover performance in the design. As described in Section 4.1, in order to complete the mission in time the *Tahr* must be capable of cruising at 296 km/h (160 kts), this results in a mission

time of 176 minutes which is just under the 180 minute limit. Figure 30a shows the power breakdown for forward flight at 1,402 m (4,600 ft.), the altitude where the majority of cruise occurs. Figure 30b shows the total power in forward flight at the mountain peak, sea level with ISA+20 and 6,000 ft. at 95°F, this shows that our rotorcraft can perform at any practical altitude and temperature. The power available is not included in figure 30b because it is not relevant since it is greater than the transmission limit at all the altitudes compared.

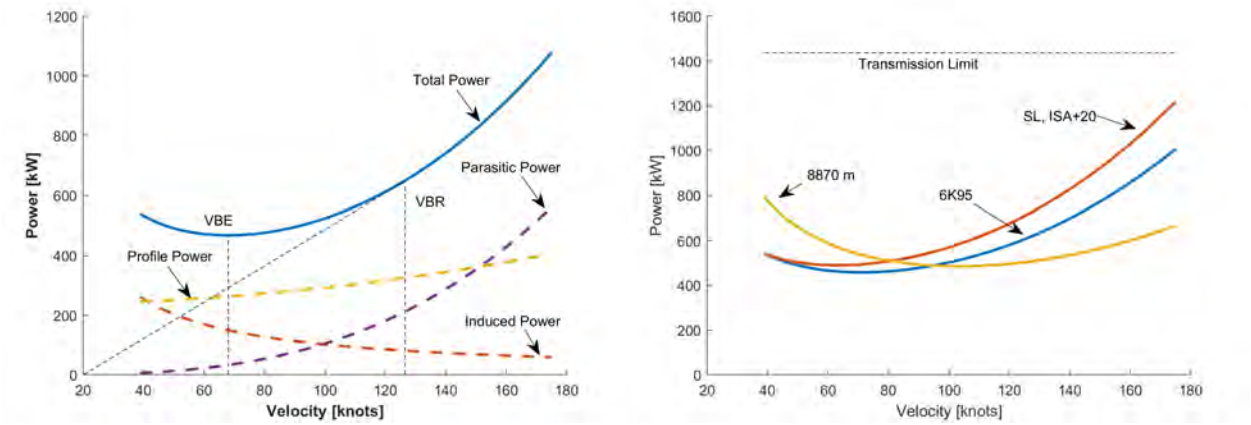

(a) Forward Flight Power Breakdown vs. Velocity

(b) Total Forward Flight Power vs. Velocity

Figure 30: Forward Flight Power Breakdown and Total Power at 3 Altitudes

In addition to breaking down the power in forward flight, Figure 30a shows the velocity of best endurance (V_{BE}) and the velocity of best range (V_{BR}) for an altitude of 1,402 m (4,600 ft.). V_{BE} is 68 knots and V_{BR} is 127 knots. The *Tahr* does not fly at these velocities throughout its mission due to time restrictions. Figures 31a and 31b show the Payload-Range and Payload-Endurance diagrams. The Payload-Range diagram is for flight at V_{BR} and the Payload-Endurance is for flight at V_{BE}. Range and endurance are increased slightly at higher altitudes due to decrease in parasitic power.

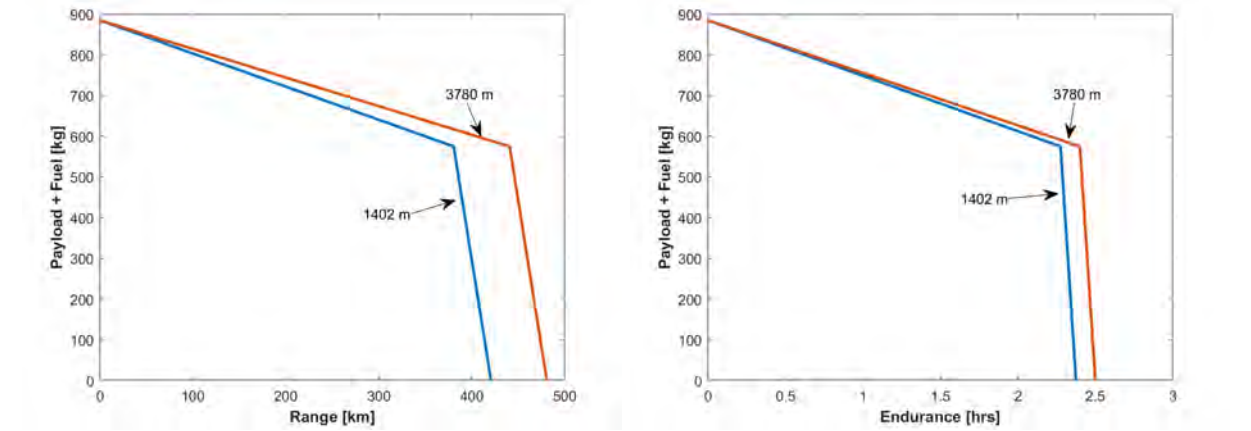

(a) Payload vs. Range

(b) Payload vs. Endurance

Figure 31: Range and Endurance at 1,402 m (4,600 ft) and 3,780 m (12,400 ft)

7.3 Climb Performance

Legs 1 and 2 begin at 1,402 m (4,600 ft.) and end at 8,870 m (29,100 ft.) at the top of Mt. Everest. In the span of three hours the helicopter needs to climb a total of 7,468 m (24,500 ft.). Because of this it is not only required that the *Tahr* maintains a high cruise speed but also a high rate of climb. In order to meet the time requirements the climb is not performed at the V_{BE}, instead the velocity is set to be 140 knots during the 1,750 ft/min rate of climb. This is only possible due to the high amount of excess power available since the helicopter sizing was based on hovering at the highest peak on earth. Figure 32 shows the rate of climb capabilities as altitude increases, we can see that the Tahr's service ceiling is 9,200 m (30,200 ft), where the rate of climb is 100 ft/min.

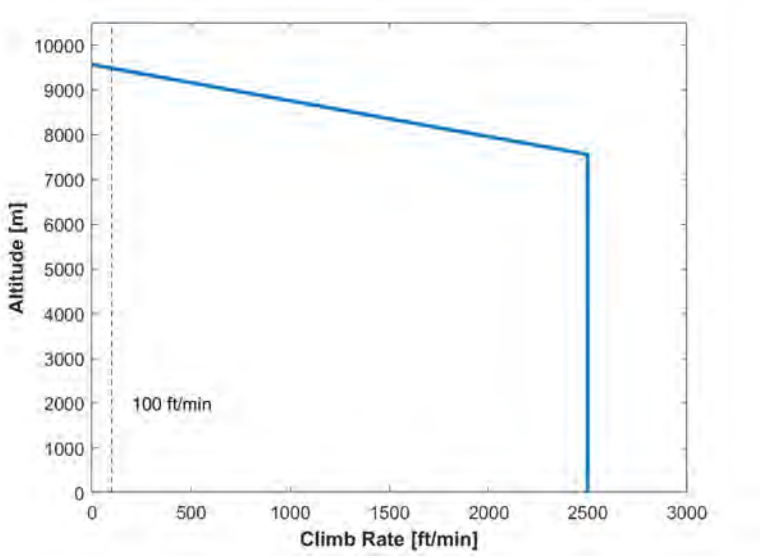

Figure 32: Altitude vs. Rate of Climb

8 Airframe Structural Design

8.1 Airframe Structure

The *Tahr's* airframe is designed to be structurally sound and spacious to allow for multi-mission capability. The structure is constructed from bulkheads, keel beams, longerons, and stringers in a semi-monocoque fashion. The main structure can be separated into three primary components: the fuselage, tail, and cowling. These components can be seen in the *Tahr* Airframe pullout.

8.1.1 Load Paths

There are two sets of load paths, one while on the ground and one while in flight.

On the ground the load is distributed along the bulkheads and is transferred directly to the landing gear. In the aft part of the airframe, the longitudinal beams transfer the load to the keel beams and upper deck beams in the fuselage and then to the landing gear via the main bulkheads.

In flight, the main loads are thrust from the main rotor and the weight of the vehicle, payload, and fuel. The load is dissipated from the main rotor shaft into lift rods via a spline connection. The lift rods are also bolted directly to the transmission housing for redundancy. They continue further to attach directly

at intersection points between the deck beams, a primary bulkhead, and a reinforcement cross beam via vibration-absorbing mounts. Figure 33 shows the diffusion of the loads in tension through the lift rods. The transmission housing is bolted directly to the steel deck below to handle torsion loads.

8.1.2 Fuselage Structure

The *Tahr's* fuselage consists of the cockpit, cabin, fuel bay, and the upper deck which contains the engine, transmission, and accessories. The structure is composed of five primary I-beam bulkheads and are connected by stringers and longerons. The base is composed of two keel beams. The fuel tank is located between the keel beams and the fuel cap is 2.5 feet high off the ground for easy refueling. The upper deck is held by the three central bulkheads and have two deck beams for added support. The transmission and engines are mounted to these deck beams in order to prevent movement.

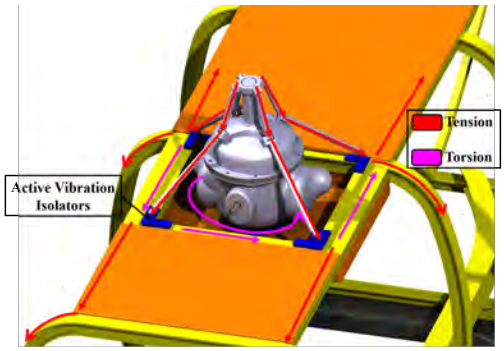

Figure 33: Load Paths for Rotor Load Diffusion

8.1.3 Tail and Empennage Structure

The tail is composed of three ring bulkheads which are supported by longitundal beams on the top and bottom of the tail structure. Longerons are used to provide additional stiffness to the tail boom. The tail is attached to the fuselage structure with the attachment bulkhead located at the aftmost section of the fuselage.

In the empennage the vertical stabilizer is separated into two sections, the upper and lower fins. The upper fin is composed of four ribs connected by spars at the quarter and three-quarter chord locations, while the lower fin is similarly composed of three ribs. The spars are connected by ring structures that are supported by the main tail logitudinal beams. The horizontal stabilizer is constructed as a singular unit for increased strength and rigidity. Nine ribs are used to transfer shear force and to maintain the airfoil shape. The ribs are connected by two spars at the quarter and three-quarter chord. The spars are connected by ring structures attached to the cantilevered tail beams.

8.1.4 Cowling Structure

The cowling for the upper deck is composed of three half-bulkheads and two ribs connected by stringers. These bulkheads are connected to the two deck beams by attachment beams.

8.1.5 Material Selection

The *Tahr's* airframe is constructed primarily out of aluminum, Kevlar/epoxy, and glass fiber/epoxy composite. The fuselage is constructed from aluminum-lithium bulkheads and the outer skin is made out of Kevlar/epoxy. The Kevlar/epoxy skin protects the helicopter from small pebbles thrown up due to the downwash of the main rotor, and aluminum-lithium provides lightweight, crashworthy structures. The nose of the cockpit is made out of glass fiber because it is transparent to radar allowing the *Tahr* to transmit signals. The bulkheads and skin of the tail and empennage are made out of Kevlar for weight and cost savings over aluminum-lithium. Because the tail is not a life-critical component, it does not need to use aluminum-lithium in its construction because it can break off in the event of a crash.

Tahr Airframe

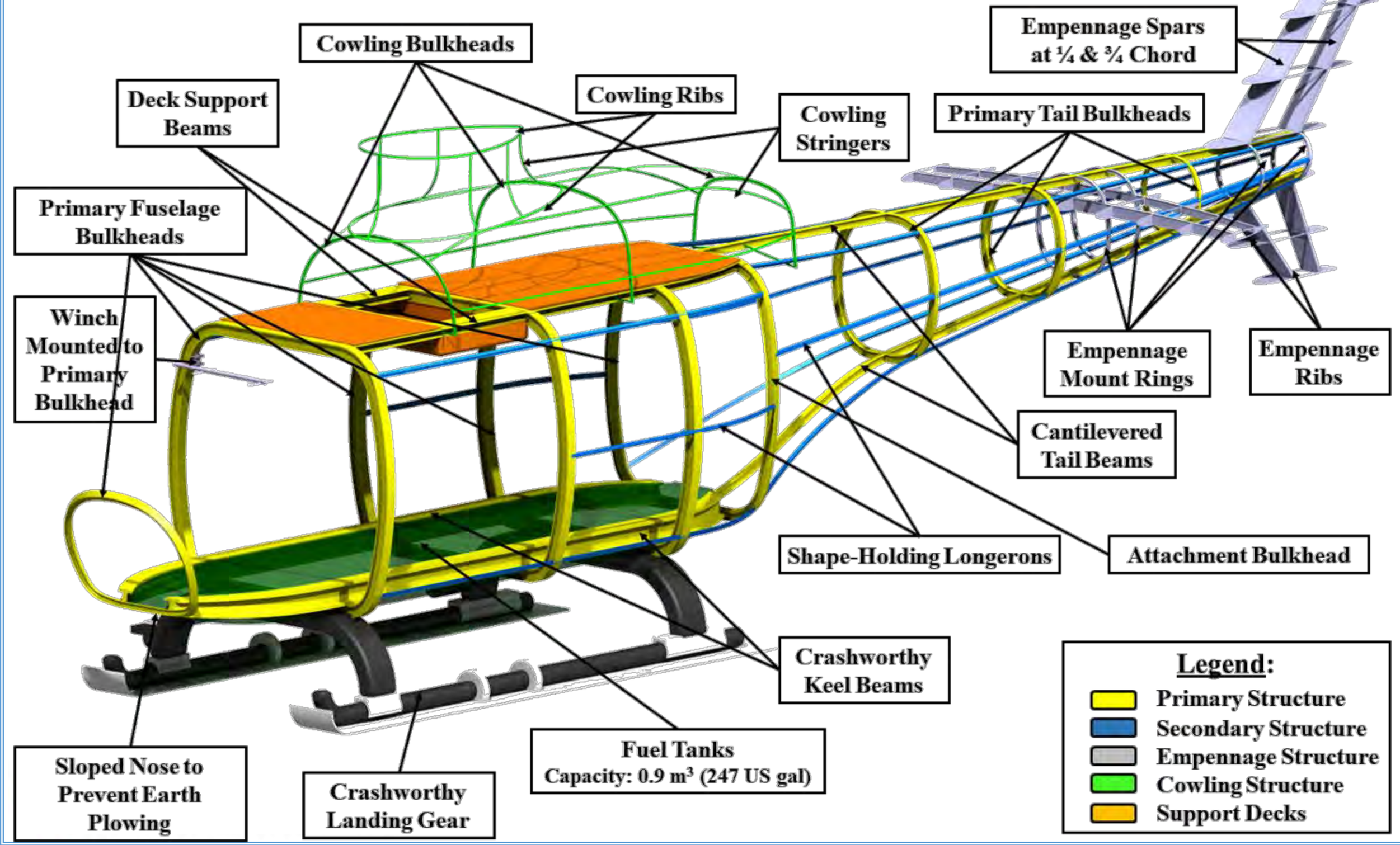

8.2 Landing Gear

During the landing gear selection process, two main considerations to the functionality were taken into account. First, the landing gear absorbs vertical energy upon impact. Second, it provides a resilient and stable suspension with the added capability of avoiding ground resonance.

8.2.1 Landing Gear Selection

The two main categories of landing gear evaluated in the design process were skid type and wheel type. Table 15 utilizes a Pugh matrix process similar to the configuration selection. Fixed skids were chosen as the baseline. Based on the criteria of weight, simplicity, drag penalty, and maintenance, it was decided to choose fixed landing gear.

Table 15: Pugh Matrix for Landing Gear Selection

Parameter	Fixed Skids	Folding Skids	Retractable Tricycle Wheeled
Mass	0	-1	-3
Simplicity	0	-2	-3
Drag Penalty	0	2	2
Crashworthiness	0	-1	-1
Maintenance	0	-1	-2
Totals	**0**	**-2**	**-7**

8.2.2 Static Stability Angles

The position of the ground contact points in relation to the center of gravity of the helicopter define two stability angles, pitch and roll. To ensure good lateral stability of the helicopter the roll stability angle must be above 60 degrees. Good pitch stability of the helicopter is ensured for more than 30 degrees. *Tahr* ensures pitch and roll stability as the roll/tip over angle is 64°, and the pitch angle 32°, Figure 34.

(a) Roll/tip over Angle of 64°

(b) Pitch Angle of 32°

Figure 34: Center of gravity envelope of *Tahr*

9 Avionics

A pilot has to perform many tasks: fly the helicopter, communicate with an array of personnel, and monitor the health of the helicopter. Because it is not easy to perform these tasks simultaneously, *Tahr* has an avionics suite that will reduce the pilot's workload. The following sections first provide an overview of the mission requirements and then present the avionics suite that addresses these challenges.

9.1 Mission Requirements

The avionics suite has been designed with the latest commercially available technology in order to reduce procurement cost while having the benefit of current technology. The mission requirements were derived based on tasks stated in the RFP.

Navigation: *Tahr* is required to navigate busy international airports and navigate its way through mountain ranges. *Tahr* must also operate in degraded visual environments, unfavorable weather that may include icing, and possibly GPS denied terrains.

Communication: The crew members should stay connected throughout the mission, including times when rescuers are outside the cabin. Beyond communication among the crew, it's possible to receive updated information from base. Arriving at busy airports, *Tahr* will communicate with air traffic control and abide by the 2020 ADS-B mandate. Lastly, it would be convenient to communicate with remote medical personnel, providing updates on the patient's status and receiving instructions regarding the optimal treatment options.

Hovering Rescue: Hoisting a patient while hovering out of ground effect (HOGE) in 74 km/hr (40 kts) winds is a challenging task, and the avionics suite should provide appropriate assistance.

9.2 Selected Avionics

The quality of the avionics suite can mean the difference between success or failure of a mission. For an extreme-altitude rescue mission, the crucial concern of gross weight demands that each instrument is carefully selected and tailored to enhance situational awareness and decrease workload. The chosen avionics closely follows a study conducted by the European Helicopter Saftey Team (EHEST) but is also tailored to the mission outlined by the RFP [9]. The technology readiness levels (TRL) of most instruments are nines, the most mature rating. The modular instrument panel permits upgrades to more advanced avionics, some of which are also mentioned. The current suite weighs a total of 200 pounds, draws 1 kW of power, and operates on 28 VDC.

9.2.1 Navigation

Tahr uses a flight management system to assist pilots in procedures such as waypoint or GPS navigation. *Tahr* obtains its current dynamics from an air data system and a redundant GPS/IMU coupled setup. Because rescues may occur in degraded visual environments or at night, *Tahr* is equipped with its bright lights, a suite for instrument meteorological conditions, and a terrain awareness system. To ensure a smooth flight for the injured, the onboard computer will highlight regions of turbulence or other inclement weather using the weather radar. Moreover, icing is carefully resolved through a combination of piezoelectrics and high efficiency heating elements.

CMA-9000 Flight Management System (FMS): The FMS helps pilots in many tasks from navigation to departure and arrival procedures. Though a touchscreen may be more intuitive, a press-button FMS decreases the likelihood of accidental presses (high levels of vibration) and provides tactile feedback [10, 11]. Furthermore, the low ambient temperatures would also require pilots to wear gloves, increasing the challenges of using touchscreen displays.

Meggitt Helicopter Air Data System (HADS): A unique swivel probe processes supplies data to the Air Data Computer, separately supplying downwash, vertical airspeed, and altitude change. See Figure 35. This system is particularly good at measuring low speed air data, crucial to a SAR mission. When combined with an inertial or GPS system, real time wind measurements can also be taken and utilized to improve rotorcraft controllability. The pilot can, at will, switch to an alternate calibrated static port per FAA requirements of single-pilot IFR. This static source will be placed beneath the cockpit of the rotorcraft.

Figure 35: Meggitt Swivel Probe and Air Data Computer

FALCN Embedded GPS/INS (EGI) and AHRS-2100: The FACLN EGI is an all-altitude precision guidance equipment that is tightly-coupled with GPS and INS to produce accurate measurements of linear and angular position, velocity, and acceleration. This EGI also supports FAA mandated ADS-B to broadcast and receive aircraft position. It provides precision guidance on approach to airports and has improved GPS signal reception in challenged environments. Two Attitude Heading Reference Systems provide redundant measurements.

Internal and External Lighting: Due to possible night-time rescue missions, the instrument panel will be illuminated with night-vision compatible lights. The cockpit and the cabin have separate lighting controls and can be isolated from one another. *Tahr* also has navigation, anti-collision, and strobe lights to improve the safety of the passenger and ground personnel. These external lights are positioned so that they do not interfering with pilots' vision. The door steps will also be illuminated to prevent missteps while entering or exiting the helicopter. A search light is gimbaled to search for hikers and to illuminate the hoisted patient.

Helicopter Terrain Awareness System (HTAWS): *Tahr*'s HTAWS has high-resolution coverage of the world's terrains and man-made obstacles. With warnings of excessive rate of descent or unsafe ground proximity, the HTWAS provides aural cues and color-coded messages on MFDs, reducing the risk of controlled flight into terrains (CFIT) during visually impaired conditions. Self-tests are conducted to avoid faulty data.

Primus 880 Weather Radar: Precipitation impairs visibility and may lead to icing. Turbulence increases vibration and decreases controllability. *Tahr* will not only display crisp images of precipitation but also evaluate the degree of turbulence, prompting pilots to avoid regions that may be uncomfortable to the patients and EMS personnel onboard.

De-Icing system: Icing is one of the limiting factors of helicopter performance. *Tahr*'s de-icing instruments were carefully selected so pilots can confidently venture into otherwise dangerous weather [12].

- **0871ND Ice Detectors**: a sensing probe resonating at natural frequency was chosen to detect ice. These sensors will be placed beneath and in the tail boom of *Tahr* near antennae. [13–16].
- **Swivel Pitot Probe**: These pitot probes will be heated for the duration of flight; an instance of failure may lead to catastrophe.
- **Cobham Antennae**: Iced antennae have decreased performances, and excessive exposure to poor weather could lead to accelerated deterioration [17, 18]. Piezo-electrics de-ice aerodynamically shaped fiberglass that protect the antennae. This method requires about 2.5 W/in^2, inexpensive compared to thermal blankets [19, 20]. Though this has not yet been rigorously proven, ultrasonics is an active field of research.
- **Astronics Windshield Heating Control**: A thin, transparent, conductive film is applied over the surface of the window. A voltage is applied to the film, which evenly distributes heat over the entire window using 5 W/in^2. This system also defogs the windshield using 1.25 W/in^2.

9.2.2 Efficient Communication

One of the challenges of piloting is managing the large amount of information ranging from arrival information to proximity warnings. *Tahr* helps the pilot organize this information with wireless intercom, programmable

aural and visual warnings (color-coded), and control over individual channels.

Figure 36: Cobham ACP

VHF-4000 and CMA-9000 Communication: In addition to two-way radio communication using the VHF-4000, the flight management system (FMS), CMA-9000, replacing congested frequencies with clear written messages, a newly introduced system known as Controller Pilot Data Link Communications (CPDLC),

JA-60 and JA-61 Wireless Intermcom System: To provide crew members with the freedom to move about during the rescue process, a wireless communication device with rechargeable batteries is included. These adapters are compatible with oxygen masks that have embedded ear and microphones.

Model 603 Aural Warning Tone Generator: This technology generates programmable aural warning tones directly to the pilot's headset, removing the hassle of reading. These tones can be managed or turned off entirely via the audio control panel (ACP). See Figure 36.

AMU-6100 Audio Management Unit (AMU): An extensive yet flexible audio management unit tailored to the pilots' preference, this light-weight system can manage up to 8 receivers and 8 transceivers. Additional channels could be used to communicate with ground crew or hospital personnel in advance of the arrival. In addition to a master control, each of the channels have individual on/off and volume control. The push release knobs provide reassuring tactile feedback. Layers of redundancy as well as a self-testing capability minimize the probability of in-flight failures. One technology that could be incorporated into the current system is 3-D audio, helping the pilots better decipher different channels, as voices are perceived to be from "different directions" [9].

9.2.3 Hover

Once victims of the accident are located, *Tahr*'s four-axis autopilot enables stable hover in winds from any azimuth as well as severe down or updrafts. Much of the instrument and sensors required for this task, such as the Attitude Heading Reference System (AHRS), are shared with other mission requirements. One built in feature of the **CMA-9000** is its approach to hover; the FMS will orient *Tahr* such that it is facing into the initial direction of wind, effectively putting *Tahr* in forward flight, improving controllability and decreasing power required [4].

KRA 405B Radar Altimeter: This light-weight altimeter provides dependable measurements of height above ground up to 2,500 ft with errors of ±3-5%.

Figure 37: Rogerson Multi-Function Displays

9.2.4 Supplemental Avionics & Supporting Equipment

Multi-Function Displays (MFDs): Electronic displays have been the lastest trend of avionics. A streamlined instrument panel design, they replace the artificial horizon, engine RPM, airspeed, etc., with an intuitive layout. Located directly in front of the pilot, these displays present vital information in a compact yet clear manner, providing everything a pilot might need in a single sweep-of-eye. See Figure 37.

Technodinamika Starter Engine and RG-390E Battery: a starter generator engine charges the RG-390E battery after the engine becomes self-sustaining. This brushless DC generator is lighter in weight, lower in maintenance cost, and longer in service life. A Nickel-Cadmium battery backs up the generator in case of a failure. This battery will supply 45 minutes of power to all essential avionics on-board, exceeding the FAA requirement of 30 minutes. Some medical equipment, such

as defibrillators, may require external electrical power supply. A larger battery could be used instead. The cold temperature will cause a decreased maximum current output; however, this current remains far above what is required.

Other Instruments: *Tahr* will have sensors and instruments mandated by the FAA to conduct instrument and visual fight (IFR and VFR). These include but are not limited to barometer readings (alternate static source included for single-pilot IFR), a magnetic direction indicator, measurements of engine RPMs and temperatures, etc. Spare fuses are available to refill the fuse board. A digital clock is included to help keep track of time. Standby instruments such as the mechanical artificial horizon will be used to navigate the helicopter if all else fails. Emergency locator transmitters are also included. Lastly, a flight data recorder retains all relevant data.

10 Rescue Mission Equipment

Rescuing the accident victim is a challenging problem. *Tahr* must first locate the hiker in possibly degraded visual environments. Hoisting an already injured hiker requires great care and effort. Lastly, *Tahr* should be prepared to provide appropriate medical attention. Organized in a similar manner as the previous, the rescue mission requirements are first discussed before elaborating on some of the specific equipment included.

10.1 Rescue Mission Requirements

Search and Rescue: Experienced hikers might carry beacons that broadcast at specific frequencies. Therefore, *Tahr* should be equipped to track these distress signals. However, *Tahr* should also be prepared to search for hikers. Once hikers are found, the rescue operation must be designed to minimize the risks of further injuries.

Pre-hospital Care: After hoisting the injured into the cabin, rescuers should aim to stabilize the patients' condition and minimize their anxiety, as it is uncommon to perform intricate procedures on the victim while in the air [21]. Therefore, *Tahr* was designed to host standard medical equipment.

10.2 Rescue Equipment

10.2.1 Streamlined Rescue

Tahr has the technology to latch onto distress beacons or scan for signs of life. An easy to use rescue litter and harness simplify the rescuer's task. Because hoists must be inspected after every mission, embedded sensors decrease maintenance time.

Figure 38: Medical Cabinet

BD406 Beacon Decoder: Hikers will often carry Personal Locator Beacons broadcasting at 121.5 or 406 MHz. This beacon decoder is able to interpret the broadcast, making hikers easy to locate. The current approved operating ceiling of this equipment is 4,500 m (15,000 ft), which should improve in the future.

Star SAFIRE 260-HLD Imaging System: This compact multi-sensor system offers high-resolution day time, low-light (infrared), and thermal imaging. See Figure 39. In the near future, convolutional neural networks (CNNs) can be trained to perform human detection, spotting hikers before rescuers can [22–24]. The camera can also be gimbaled to observe the hoist operation and tailrotor position.

RECCO Rescue System: The RECCO system can detect people who are buried underneath the snow or have fallen into a crevasse, where cameras or thermal techniques are ineffective. The range is 650 ft (200 m) through air and 100 ft (30 m) through snow.

Helitack AirBag and Response Harness: A light-weight and durable litter, the Helitack AirBag is very

easy to use with its color-coded buckles and is conveniently stored in tight spaces. The Response Harness is included for those who are not critically injured.

Goodrich Pegasus Hoist: The Pegasus hoist is tailored to alleviate pendulum motion and reduce wear. Its monitoring system records load, speed, cycle and other information to expedite post-mission inspection. The line-replaceable units can be exchanged in the case of malfunctions.

10.2.2 Pre-hospital Care

The cabin of *Tahr* was designed to imitate the interior of an ambulance, increasing EMS personnel work space and cleverly making room for storage. The expected on-board medical equipment were based on well-known high altitude conditions and were prepared for the worst of injuries. All medical equipment is located in the medical cabinet which can be seen in Figure 38

Medical Floor: Customized medical floor ensure that stretchers remain in place. This floor is also easily sanitized so *Tahr* is ready for the next rescue mission. Furthermore, the floor can be removed component by component with relative ease so that *Tahr* can fulfill other mission profiles.

Medical Package: Tahr is designed to accommodate the medical equipment required for advanced life support (ALS) [25]. Basic life support (BLS) include an adequate source of oxygen, bag-valve masks, hemorrhage control supplies, control of breathing, etc. ALS augments this package with capabilities such as cardiac monitoring, resuscitative medication, CO_2 monitoring, etc. [25]. *Tahr* is prepared to handle known illnesses ranging from frostbite to severe acute mountain sickness (AMS) [26–28].

Figure 39: Star SAFIRE 260-HLD Imaging System

11 Concept of Operations (CONOPS)

Using input from Air Zermatt search and rescue, the team was able to develop a concept of operations to be used for a search and rescue mission. The Concept of Operations Foldout shows a visual of the RFP mission profile.

There are two passengers in need of rescue on a mountain at 8,870 m (29,100 ft). One is assumed to be in critical condition and unconscious. The *Tahr* must mobilize in a short period of time, reach the rescuees, and return to a medical facility within three hours. For both scenarios the co-pilot's seat is able to swivel around so that he is able to access the cabin, as the copilot is specified as being the EMS worker.

Figure 40: Swiveling Co-Pilot Seat

Concept of operations – Mission Profile

1. d	2.g	3.d
Land 2 min hover 20 minutes for refuel 10% fuel margin	Land 2 min hover 10% fuel margin	Land 2 min hover 10% fuel margin

1. c
Level cruise for 135 km (84 miles)
(~ 30 min: 296 km/h (160 kts))

1. b
Climb to 3,780 m
(12,400 ft)

1. a
Take off
Payload: 3crew+150 kg
= 405 kg (893 lb)
2 min hover

2.b
Climb to 8,870 m
(29,100 ft)

2.c
Level cruise for 28 km (17.4 miles)
(~ 6 min: 296 km/h (160 kts))

2.d
HOGE for 30 min
Payload: 405 kg + 2PAX = 575 kg
(1,268lb)

Mountain Peak : **8,870m (29,100ft)**

2. a
Take off
2 min hover

1. d

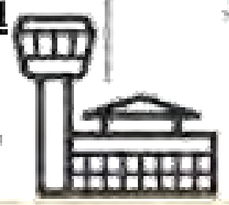

2.e
Descent to 3,780 m
(12,400 ft)

2.f
Level cruise for 28 km (17.4 miles)
(~ 6 min: 296 km/h (160 kts))

2.g

Small Airport: **3,780m (12,400 ft)**

3.b
Descend to 1,402 m
(4,600ft)

3. a
20 minutes for refueling
Take off
2 min hover

3.c
Level cruise for 135 km
(84 miles)

3.d

International Airport: **1,402 m (4,600 ft)**

Leg 1	~52 min
Leg 2	~72 min
Leg 3	~52 min

UNIVERSITY OF MARYLAND

11.1 Normal Flow of Events

1. At reception of the distress call the pilot, co-pilot/EMS worker, and rescue worker are notified and prepare for flight. The *Tahr* is checked and cleared for flight. Take-off occurs within 5 minutes during the day and 20 minutes at night.
2. From the international airport, the *Tahr* flies to a nearby smaller airport to refuel.
3. The *Tahr* flies from the smaller airport to the location of the rescuees.
4. Hovering over the location, the hoist is swung out of the open cabin door and the rescue worker is lowered with the litter. Once he reaches the ground the helicopter goes to hover in a location where the downwash will not affect the process but is still within communication range.
5. Once the injured rescuee is safely strapped to the litter the *Tahr* will return to lift him up with the rescue worker. The process is repeated for the second rescuee.
6. The *Tahr* flies back to the small airport to refuel again, then flies to the international airport. During this flight medical aid will be provided to the injured rescuee(s).
7. The *Tahr* will land at the international airport and the rescuees will be taken to a hosptial for further medical care.

11.2 Alternate Flow of Events

1. At reception of the distress call the pilot, co-pilot, and EMS worker are notified and prepare for flight. The *Tahr* is checked and cleared for flight. Take-off within 5 minutes during the day and 20 minutes at night.
2. From the international, airport the *Tahr* flies to a nearby smaller airport to refuel.
3. The *Tahr* flies from the smaller airport to the location of the rescuees.
4. The *Tahr* will perform a soft landing near the rescuees after the pilot determines it is safe to do so. The rescuees will be loaded into the helicopter.
5. The *Tahr* flies back to the small airport to refuel again, then flies to the international airport. During this flight medical aid will be provided to the injured rescuee(s).
6. The *Tahr* will land at the international airport and the rescuees will be taken to a hosptial for further medical care.

12 High Altitude Tradeoffs

12.1 Versatile Performance

In order to meet the hover requirements in the RFP, it was important to design a very large and powerful rotor. Additionally, the engines have to produce large amounts of power to overcome the low density at high altitude. What results is a rotorcraft which has very high performance specs at typical altitudes. This lends *Tahr* to being able to accomplish many high performance tasks. Table 16 explains some of the unique effects such high altitude has on the mission.

As the *Tahr* was designed for extreme high altitude, it is well-suited for military missions at 6k95. Potential mission profiles are troop resupply, search and rescue, and covert operations as the noise signature is very low. In addition to military uses, *Tahr* would also be an effective in paramilitary or other policing applications.

The *Tahr's* low downwash would make it a safe and effective firefighting rotorcraft. *Tahr* could deliver the water to the fire without heavy downwash fanning the flames. As a rotorcraft, it can also change over to

Table 16: Pros and Cons of Effects of High Altitude

Effects	**Pros**	**Cons**
Low Density	Low perceived downwash, Lower drag - better profile and parasitic performance	Poor air breathing engine performance
Low Temperature	Raises density, Lowers overheating risk	Reduces the risk of engine overheat
High Winds	Tailwinds increase cruise speed	Lowered aircraft stability
Lower Speed of Sound	None	Tip speed closer to transonic region
Low Oxygen	None	Risk for hypoxia

search and rescue as fire conditions change. In the past, firefighter fatalities have occurred because fixed wing aircraft were used for firefighting. Sudden wind changes then cut off the firefighters' escape routes and there were no rescue helicopters in the area.

Figure 41: *Tahr's* Versatility

Tahr's cruise speed and low noise make it an ideal candidate for executive travel. What gives *Tahr* such an advantage for this is the large blades on the rotor which give off lower frequency noise. This makes for a quieter vehicle and passengers would be able to carry on a conversation without raising their voices.

As the *Tahr* was designed with good control authority it would operate smoothly in high wind environments such as wind turbine or cell tower maintenance missions. Figure 41 shows how the *Tahr* could be configured for many alternate mission profiles.

13 Flight Mechanics

From entering congested airspace at busy international airports to navigating mountainous terrains in degraded visual environments, pilots must be on high alert at all time. During a helicopter emergency medical service (HEMS) as proposed in the RFP, one challenge in particular is the hoisting of the injured hiker. With winds up to 74 km/hr (40 knots) from any azimuth, not only will the rotorcraft struggle to hover at one point, the injured hiker will spin and oscillate.

13.1 Overview of Dynamics

Helicopters commonly carry underslung loads, whether firefighting, installing ski lifts, or transferring supplies between ships, etc. Traditionally, the oscillation of underslung load is simply managed by the pilot. However, this section discusses studies of oscillating slung-loads and implications for the dynamics of *Tahr*.

Simplifying the problem setup for use in a laboratory setting, Potter, Adams, and Singhose established a three degree-of-freedom model that captures the linear translation of the fuselage, the pitching of the fuselage, and the in-plane pendulum of the slung-load [29]. Nagaraj and Chopra proposed an underslung rescue module and three different types of control to minimize slung-load pendulum motion [30]. Fusato, Guglieri, and Celi studied the handling qualities of an articulated rotor helicopter with slung-load for cables between five to eight meters and weight ratios up to 28% [31].

One notable parameter was the ratio between the slung-load mass and helicopter mass. For a slung-load that is 3-5% of *Tahr*'s gross weight, the dynamics should not be heavily impacted.

Although the underslung load does not alter the dynamics, *Tahr* operates in a harsh environment of high winds and degraded visibility. Thus, *Tahr* will be equipped with a Stability Augmentation System (SAS) and an Automatic Flight Control System (AFCS). Together, they will assist the pilot in holding altitude, attitude and heading.

13.2 Center of Gravity Analysis

It is crucial to maintain a consistent center of gravity (COG) throughout the mission. This is a parameter closely coupled to the handling qualities of the rotorcraft. To ensure *Tahr* retains reasonable handling qualities despite the shifts in COG, a center of gravity analysis was conducted. Throughout the mission, there a few notable sources of shifts in COG:

- Rescue personnel moving about the cabin
- Door sliding open for rescue
- Hoisting injured hikers
- Fuel burn

Fuel will be used in a manner such that the COG is not significantly shifted. Nonetheless, decrease in the total mass due to fuel burn implies that the COG is more prone to shifting. The largest lateral shift in COG occurs when the hoist is maximally loaded. The largest shift in longitudinal COG would be when both injured hikers are in their gurneys and rescue personnel have gathered near the rear of the cabin.

14 Flight Controls

Tahr has a complete suite of sensors (Section 9) to describe the surrounding environment and capture its current state. These data are combined with pilot inputs and translated into commands for mechanical actuation. The hoist operator will lessen the oscillation of the hoisted patient; this method is both simple and cost-effective.

14.1 Pilot Control

Tahr was designed with standard cockpit controls. The linkage from pilot input to control surfaces is entirely mechanical. A fly-by-wire system was considered, but as the technology is not yet mature, a simple mechanical system was used instead.

The pilot uses the flight management system for long-term navigation and the autopilot control panel for in-flight control. The multi-function displays shown in Figure 42 will highlight the autopilot modes currently selected.

14.2 Sensors, Actuators, and Autopilot Control Panel

Tahr's accelerometers and gyroscopes are located near the center of mass for the most accurate data. It also has multiple pitot tubes and two air data computers. Control surfaces are managed by hydraulic actuators [32].

The autopilot minimizes the workload of the pilot. The SAS can be engaged during hover to low-speed flight to provide short-term stabilization. An attitude retention mode manages the pitch and roll of the rotorcraft, allowing pilots to remove their hands from the control. A position hold will be included to simplify hovering during rescue. Moreover, the autopilot can be disengaged if failure occurs mid-flight, when *Tahr* can be flown manually.

Figure 42: *Tahr's Cockpit Console*

15 Acoustics

FAA Stage 3 helicopter noise certification standards are limited to 86 EPNdB during take-off, 84 EPNdB during flyover, and 89 EPNdB during approach. Furthermore, given an aircraft over 1418 kg, regulation adds 3.0 EPNdB to each of the three requirements per doubling of $\log(Weight)$, [33]. However, the acoustic analysis on the *Tahr* resulted in values in Sound Pressure Level (SPLdB).

15.1 FAA Noise Requirements

FAA states that time-critical missions are noise-excusable public services. However, the *Tahr* was designed with a minimal acoustic signature for the underslung patient, following an analysis based on SPL explained below as well as alternative missions, such as executive travel.

The acoustic signature of *Tahr*'s main rotor was analyzed using an in-house acoustics code based on the Ffowcs Williams-Hawkings equations, [34]. SPL was calculated for both thickness and loading noises in hover and cruise conditions. Thickness noise is a result of the displacement of the fluid and loading noise is due to aerodynamic loading. The former results from blade thickness and propagates in the rotor plane, while the latter is due to lift and drag and propagates below the rotor. In the code, blade thickness and slope determine the thickness noise while loading noise is computed by normal and chordwise forces on the blade.

15.2 Acoustic Analyses

For each loading case, the acoustics signature is presented for a hemisphere surrounding the helicopter and a circle at ground level (150m below the plane of the rotor at sea-level and 63m below the plane of the rotor

at rescue altitude). The figure axes are normalized by the rotor radius. Two scenarios were considered: (1) cruise and hover at 150m (492 ft) as specified by the FAA noise regulation, and (2) hover at 8,870 m (29,100 ft) as specified by the RFP.

15.2.1 Sea Level Altitude

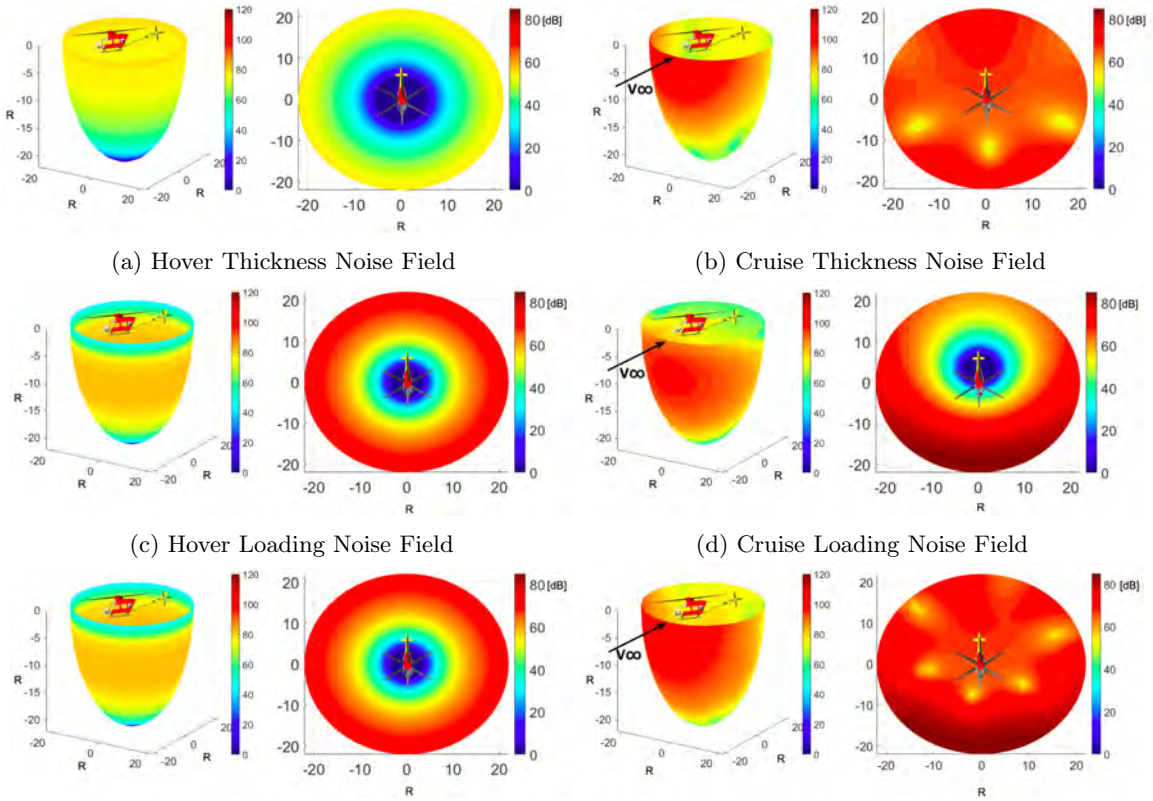

(a) Hover Thickness Noise Field

(b) Cruise Thickness Noise Field

(c) Hover Loading Noise Field

(d) Cruise Loading Noise Field

(e) Hover Total Noise Field

(f) Cruise Total Noise Field

Figure 43: Acoustic Analysis at Sea Level Altitude

Figure 43 shows the predicted acoustics at sea level. Due to the Doppler effect in forward flight, wavelength decreases in front of and increases behind the helicopter. Because the perceived noise will change in pitch as the object passes, there are asymmetries as seen in Figures 43b, 43d and, 43f.

The thickness noise is dependent on surface slope airfoil thickness and velocity. Therefore, the thickness noise in cruise is higher than in hover as shown in Figures 43b and 43a. The loading noise in Figure 43d is higher than in 43c due to the higher chordwise loading in the cruise condition. Overall, the noise levels of *Tahr* in both hover and cruise comply with the FAA standards.

15.2.2 Mission Altitude, 8,870 m (29,100 ft)

Figure 44 shows the noise during rescue, during which *Tahr* maintains a suitable acoustic environment for the patients. Table 17 summarizes the maximum noise levels on the circular planes located at 150 and 61 meters, respectively, below the aircraft.

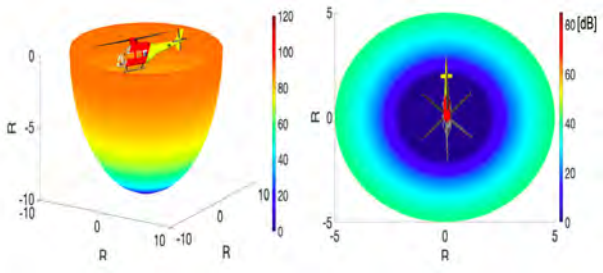

(a) Rescuing Thickness Noise Field

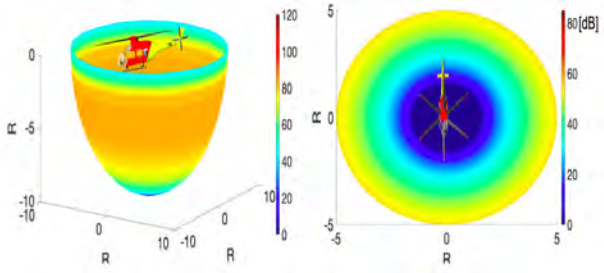

(b) Rescuing Loading Noise Field

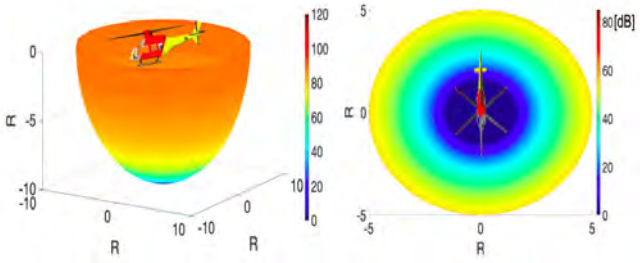

(c) Rescuing Total Noise Field

Figure 44: Acoustic Analysis at Mount Peak

Table 17: Maximum Noise Level on Ground with *Tahr* 150 and 61 Meters Above

Noise (SPLdB)	**Hover SL**	**Cruise SL**	**Hover Rescue**
Thickness	54.06	76.38	42.09
Loading	72.06	86.36	55.18
Total	72.10	86.39	55.19

16 Cost

Cost estimations of *Tahr* follow models of NDARC (NASA Design and Analysis of Rotorcraft), statistical models based on existing databases. The total cost of an aircraft includes purchase, operations, and maintenance costs. Each type of cost is then further divided into more specific categories.

The aircraft purchase cost consists of airframe, mission equipment, and flight electronics costs. Equation 2 describes the airframe cost coefficients in \$/kg, which is multiplied by the airframe weight to obtain the airframe cost.

$$c_{AF} = 739.91 K_{ET} K_{EN} K_{LG} K_R W_{AF}^{1.0619} (P/W_{AF})^{0.5887} N_{blade}^{0.1465} \tag{2}$$

The definitions of the coefficients are as follows.

- K_{ET} - Engine Type
- K_{EN} - Number of Engines
- K_{LG} - Landing Gear Type
- K_R - Rotor Type
- W_{AF} - Weight of airframe (lbs)
- P - Power (hp)
- N_{blades} - Number of Blades

The purchase cost of the *Tahr* was estimated to be \$11.4 Million. In a similar manner, the maintenance cost was estimated to be \$719.67 per hour. These costs also account for a 1.74 inflation factor using the

Consumer Price Index and extrapolating between 1994 and 2019. The cost was also validated using 2019 purchase costs of 3 Airbus helicopters.

To minimize cost, engines were chosen off-the-shelf to eliminate cost of modification; only mission critical avionics were incorporated. To reduce operational costs, *Tahr*'s rotor blades and fuselage were optimized for hover and forward flight in the extreme conditions specified by the RFP. Moreover, *Tahr* has embedded sensors and line-replaceable units to expedite maintenance. Lastly, *Tahr*'s equipment have high technology readiness levels to reduce testing and certification costs.

17 Weight Breakdown

For a rotorcraft operating at extreme altitudes, the *Tahr* is designed to be as light-weight as possible. As seen in Table 18, the heaviest group of the *Tahr* are the rotor assembly, gearbox, the bulkheads, and the turbine engines. Ultimately, the weight breakdown in this section matches the estimated MTOW in section 3.3, using the method explained in section 3.1.

Table 18: *Tahr* Weight Breakdown

		Weight (lb)	Weight (kg)	% Empty Weight
Rotor Group	Blade Assembly	544.0	246.8	8.73
	Hub & Hinge	469.2	212.8	7.53
Tail Group	Horizontal Stabilizers	22.0	10.0	0.35
	Vertical Stabilizer	44.1	20.0	0.71
	Tail Rotor Blades	66.1	30.0	1.06
	Tail Rotor Hub & Hinge	50.7	23.0	0.81
	Tail Boom	132.3	60.0	2.12
Fuselage Group	Bulkheads (Fuselage Structure)	617.3	280.0	9.90
	Door	110.2	50.0	1.77
	Window	44.1	20.0	0.71
	Skin	66.1	30.0	1.06
	Paint	20.0	9.1	0.32
Drive System	Gear Box	573.2	260.0	9.20
	Drive Shaft	101.4	46.0	1.63
	Tail Rotor Drive Shaft	110.2	50.0	1.77
Landing Gear Group	Landing skids	255.7	116.0	4.10
	Landing skis	88.2	40.0	1.41
Propulsion Group	Primary Engines	1023.6	464.3	16.42
	Battery	62.1	28.0	0.99
	Starting System	35.3	16.0	0.57
	Exhaust System	200.0	90.7	3.21
	Firewalls	81.8	37.1	1.31
	Engine Cowl	292.1	132.5	4.69
	Lubrication System	50.0	22.7	0.80
	Fuel System	26.7	12.1	0.43
Avionics Group	Flight Instrument	203.7	92.4	3.27
	De-icing group	17.0	7.7	0.27
	Connections (wires, bolts)	30.0	13.6	0.48
Flight Control Group	Rotor Controls	330.7	150.0	5.31
	Cockpit Control	154.3	70.0	2.48
Equipment Group	Seats	132.3	60.0	2.12
	Camera & Search Light	115.0	52.2	1.85
	Hoist & Litter	133.1	60.4	2.14
	Oxygen	30.0	13.6	0.48
Empty Weight		6232.3	2826.9	100.00
Payload	Crew	551.2	250.0	-
	Passenger	374.8	170.0	-
	Fuel	683.4	310.0	-
	EMS Equipment	330.7	150.0	-
Gross Weight		8172.4	3706.9	-

References

[1] Tishchenko, M. and Nagaraj, V.T. *ENAE634 Helicopter Design Lecture Notes*. 2008.

[2] Johnson, W. *NASA Design and Analysis of Rotorcraft*. Tech. rep. NASA/TP–2009-215402. Moffet Field, CA: NASA Ames Research Center, Jan. 2011.

[3] Johnson, W. *NDARC — NASA Design and Analysis of Rotorcraft Validation and Demonstration*. Tech. rep. Moffet Field, CA: NASA Ames Research Center, 2010.

[4] Nagaraj, V. T., Govindarajan, B. M., and Chopra, I. "Preliminary Design of Rotorcraft". Unpublished.

[5] Young, J.E. "Helicopter Vertical Stabilizer Design Considerations". MA thesis. Montery, California: Naval Postgraduate School, June 1983.

[6] Varga, Béla. "Power Sources of Military Helicopters". In: *Atlantic Association for Research in the Mathematical Sciences (AARMS)* 17.2 (2018), pp. 139–168.

[7] Guo, Y et al. "Analytical Formulation for Sizing and Estimating the Dimensions and Weight of Wind Turbine Hub and Drivetrain Components". In: *National Renewable Energy Laboratory* (June 2015).

[8] Shigley, J. E., Nisbett, J. K., and Budynas, R. G. *Shigley's Mechanical Engineering Design 9th Edition*. McGraw-Hill, 2011.

[9] Stevens, J.M.G.F. and Vreeken, J. *The Potential of Technologies to Mitigate Helicopter Accident Factors–An EHEST Study*. Tech. rep. Amsterdam, The Netherlands: National Aerospace Laboratory, Oct. 2014.

[10] Rouwhorst, W. et al. "Use of Touch Screen Display Applications for Aircraft Flight Control". In: *2017 IEEE/AIAA 36th Digital Avionics Systems Conference (DASC)*. St. Petersburg, FL, 2017. DOI: 10.1109/DASC.2017.8102060.

[11] Gauci, J. et al. "Design and Evaluation of a Touch Screen Concept for Pilot Interaction with Avionic Systems". In: *2015 IEEE/AIAA 34th Digital Avionics Systems Conference (DASC)*. Prague, Czech Republic, 2015. DOI: 10.1109/DASC.2015.7311398.

[12] Goraj, Z. "An Overview of the Deicing and Antiicing Technologies with prospects for the Future". In: *24TH International Congress OF THE Aeronautical Sciences*. Yokohama, Japan, 2004.

[13] Bassey, C. E. and Simpson, G. R. "Aircraft Ice Detection using Time Domain Reflectometry with Coplanar Sensors". In: *2007 IEEE Aerospace Conference*. Big Sky, MT, 2007. DOI: 10.1109/AERO.2007.352857.

[14] Akhloufi, M. and Benmesbah, N. "Outdoor ice accretion estimation of wind turbine blades using computer vision". In: *2014 Canadian Conference on Computer and Robot Vision*. Quebec, Cananda, 2014. DOI: 10.1109/CRV.2014.41.

[15] Gao, H. and Rose, J. L. "Ice Detection and Classification on an Aircraft Wing with Ultrasonic Shear Horizontal Guided Waves". In: *IEEE Transactions on Ultrasonics, Ferroelectrics, and Frequency Control* 56 (2 Feb. 2009). DOI: 10.1109/CRV.2014.41.

[16] Flatscher, M., Neumayer, M., and Bretterklieber, T. "Field Sensor Analysis for Electrical Impedance Spectroscopy Based Ice Detection". In: *2017 IEEE Sensors*. Glasgow, UK, 2017. DOI: 10.1109/ICSENS.2017.8234035.

[17] Haller, G. L. "Icing of Aircraft Antenna Wires". In: *Journal of Aeronautical Sciences* 6 (Nov. 1938), pp. 27–28.

[18] O'Keefe, K. et al. "Effect of Ice Loading of a GPS Antenna". In: *Proceedings of the 1999 National Technical Meeting of The Institute of Navigation*. San Diego, CA, 1999, pp. 861–869.

[19] DiPlacido, N., Soltis, J., and Palacios, J. "Enhancement of Ultrasonic De-Icing via Tone Burst Excitation". In: *Journal of Aircraft* 53 (6 Dec. 2016). DOI: 10.2514/1.C033761.

[20] Overmeyer, A., Palacios, J., and Smith, E. "Ultrasonic De-Icing Bondline Design and Rotor Ice Testing". In: *Journal of Aircraft* 51 (12 Dec. 2013). DOI: 10.2514/1.J052601.

[21] Prabhakar, M., Kampani, G., and Chandna, A. *Air Ambulance Services Transport of Critically Sick Patients*. Tech. rep. The Association of Physicians of India.

[22] Dalal, N., Triggs, B., and Schmid, C. "Human Detection Using Oriented Histograms of Flow and Appearance". In: *European Conference on Computer Vision*. Graz, Austria, 2006, pp. 428–441.

[23] Schwartz, W. R. et al. "Human Detection Using Partial Least Squares Analysis". In: *2009 IEEE 12th International Conference on Computer Vision*. Kyoto, Japan, 2009. DOI: 10.1109/ICCV.2009.5459205.

[24] Tuzel, O., Porikli, F., and Meer, P. "Human Detection via Classification on Riemannian Manifolds". In: *2007 IEEE Conference on Computer Vision and Pattern Recognition*. Minneapolis, MN, 2007. DOI: 10.1109/CVPR.2007.383197.

[25] *Eleventh Edition Accreditation Standards of the Commission on Accreditation of Medical Transport Systems*. Tech. rep. Sandy Spring, SC: Commission on Accreditation of Medical Transport Systems, July 2018.

[26] Sutherland, A. *Why are so many people dying on Everest?* 2006.

[27] Imray, C., Grieve, A., and Dhillon, S. "Cold damage to the extremities: frostbite and nonfreezing cold injuries". In: *Postgraduate Medical Journal* 85 (May 2009), pp. 481–488.

[28] Smedley, T. and Grocott, M. PW. "Acute high-altitude illness: a clinically oriented overview". In: *British Journal of Pain* 7 (2 May 2013), pp. 85–94.

[29] Potter, James, Adams, Christopher, and Singhose, William. "A Planar Experimental Remote-Controlled Helicopter With a Suspended Load". In: *IEEE/ASME Transaction on Mechatronics* 20.5 (Oct. 2015), pp. 2496–2503. DOI: 10.1109/TMECH.2014.2386801.

[30] Nagaraj, V. T. and Chopra, I. "Design of a Helicopter Urban Disaster Rescue Module". In: *64th Annual Forum of the American Helicopter Society*. Montreal, Canada, 2008.

[31] Fusato, D., Guglieri, G., and Celi, R. "Flight Dynamics of an Articulated Rotor Helicopter with an External Slung Load". In: *55th Annual Forum of the American Helicopter Society*. Montreal, Canada, 1999.

[32] *Student Handout: UH-60 Flight Control and Hydraulic Systems*. Tech. rep. United States Army Aviation Center, July 2002.

[33] (FAA), Federal Aviation Administration. *Details on FAA Noise Levels, Stages, and Phaseouts*. 2016.

[34] Williams, J. F. and Hawkings, D. L. "Sound generation by turbulence and surfaces in arbitrary motion". In: *Phil. Trans. R. Soc. Lond. A* 264 (May 1969), pp. 321–342.